

Kinematic Properties and Stellar Populations of Faint Early-Type Galaxies. II. Line-Strength Measurements of Central Coma Galaxies

A. Matković

Astronomy Department, University of Florida, P.O. Box 112055, Gainesville, FL 32611, USA

R. Guzmán

Astronomy Department, University of Florida, P.O. Box 112055, Gainesville, FL 32611, USA

P. Sánchez-Blázquez

Centre for Astrophysics, University of Central Lancashire, PR1 2HE, Preston, UK

J. Gorgas and N. Cardiel

Departamento de Astrofísica, Facultad de Físicas, Universidad Complutense de Madrid, Ciudad Universitaria, 28040 Madrid, Spain

N. Gruel

Astronomy Department, University of Florida, P.O. Box 112055, Gainesville, FL 32611, USA

ABSTRACT

We present line-strength measurements for 74 early-type galaxies in the core of the Coma cluster reaching down to velocity dispersions, σ , of 30 km s^{-1} . The index- σ relations for our sample, including galaxies with $\sigma < 100 \text{ km s}^{-1}$ (low- σ), differ in shape depending on which index is used. We notice two types of relations for the metallic indices: one showing a break in the slope around $\sim 100 \text{ km s}^{-1}$, and another group with strong linear relations between an index and $\log \sigma$. We find no connection between the behavior of index- σ relations with either α - or Fe-peak elements. However, we find indications that the relations are tighter for indices which do not depend on the micro-turbulent velocities of stellar atmospheres. We confirm previous results that low- σ galaxies including dE/dS0s are on average younger, less metal rich, and have lower $[\alpha/\text{Fe}]$ in comparison to E/S0s. Our data show that these trends derived for high- σ galaxies extend down to dE/dS0s. This is a factor of ~ 2 lower in σ than previously published work. We confirm that the observed anti-correlation between age and metallicity for high- σ galaxies is consistent with the effects of correlated errors. Low- σ galaxies also show a similar relation between age and metallicity as a result of correlated errors. However, they are offset from this relationship so that, on average, they are less metal rich and younger than their high- σ counterparts.

Subject headings: galaxies: abundances — galaxies: clusters: individual (Coma) — galaxies: dwarf — galaxies: elliptical and lenticular, cD

1. INTRODUCTION

The “classical” view of the formation of massive early-type galaxies is that they formed relatively fast at early redshifts, and that they evolved passively. This is supported by tight scaling relations that these galaxies exhibit. However, the question of how their low mass counterparts, dwarf early-type (dEs/dS0s) galaxies, formed remains unanswered.

One of the ways to investigate the star formation histories of early-type galaxies is through their line-strength indices which, when combined with stellar population models (SPM), yield ages and metallicities. However, the process of deriving star formation histories of galaxies by comparing line-strengths with models is complicated by the degeneracy between age and metallicity (Worthey 1994), abundance ratio differences between the calibration stars used to calculate the models and the galaxy spectra, and strong Balmer lines which can be caused by either young stellar populations or an extended horizontal branch.

The most recent studies have incorporated iterative procedures and/or simultaneous fitting of as many indices as possible while deriving ages, metallicities and relations between the line strengths and velocity dispersions (σ) of early-type galaxies (Proctor et al. 2004; Thomas et al. 2005; Nelan et al. 2005; Denicoló et al. 2005; Sánchez-Blázquez et al. 2006a,b). Despite these improved techniques and larger samples extending to lower luminosities, we still do not have a clear picture of the star formation histories of early-type galaxies, especially at the low mass end.

It is well known that lower-luminosity early-type galaxies show a wider range in age than their more luminous counterparts (e.g. Caldwell 1983; Bender et al. 1993; Worthey & Ottaviani 1997; Kuntschner & Davies 1998; Poggianti et al. 2001a; Caldwell et al. 2003). Some studies find that the lower mass galaxies also display younger ages (Poggianti et al. 2001a; Caldwell et al. 2003; Proctor et al. 2004; Thomas et al. 2005; Nelan et al. 2005), while others do not find this relation, or find that it depends on environment (Trager et al. 2000b; Kuntschner et al. 2001; Sánchez-Blázquez et al. 2006a). Similarly a number of studies show that lower mass galaxies have lower metallicities (Brodie & Huchra 1991; Poggianti et al. 2001a;

Kuntschner et al. 2001; Mehlert et al. 2003; Proctor et al. 2004; Nelan et al. 2005; Thomas et al. 2005; Sánchez-Blázquez et al. 2006b; Bernardi et al. 2006). Further, these galaxies display lower (closer to solar) abundance of α -elements than the luminous elliptical galaxies (Es) which have an overabundance of α -elements when compared to the values in the solar neighborhood (Gorgas et al. 1997; Jorgensen 1997; Trager et al. 2000b; Nelan et al. 2005; Thomas et al. 2005; Denicoló et al. 2005; Bernardi et al. 2006; Sánchez-Blázquez et al. 2006b). The lower values for the abundance ratio, α/Fe , for low-mass galaxies suggests that these galaxies have had more extended star formation histories than their massive counterparts.

The main goal of this project is to characterize internal kinematics and stellar populations of dE/dS0 galaxies as a function of cluster environment. In Matković & Guzmán (2005, hereafter Paper I) we described the internal kinematics of these galaxies in the dense central region of the Coma cluster. Here (paper II) we investigate the properties of the underlying stellar populations of these galaxies. The following papers will examine the same properties of these galaxies in a region SW of the cluster center, just outside the virial core, and will investigate how the location within the cluster affects these properties. Currently, there are only a few other studies which include dE/dS0 galaxies in their samples. While these studies reach $\sigma \approx 50 \text{ km s}^{-1}$ (Poggianti et al. 2001a; Caldwell et al. 2003; Nelan et al. 2005; Sánchez-Blázquez et al. 2006a), we present a statistically representative number of dE/dS0s in Coma reaching $\sigma = 30 \text{ km s}^{-1}$. In this paper, we investigate trends between the Lick/IDS line-strengths and σ and determine mean luminosity-weighted ages, metallicities and α/Fe ratios for a sample of 74 early-type galaxies in the central part of the Coma cluster. In §2 we describe our sample selection and our spectroscopic data; §3 describes the absorption line strength measurements; in §4 we compare our measurements with other authors; in §5 we investigate the relations between different indices and σ ; §6 describes the ages, metallicities and α -ratios.

2. SAMPLE SELECTION AND SPECTROSCOPIC DATA

We observed spectra of bright and faint early-type galaxies in two different environments within the Coma cluster, the central $20' \times 20'$ and a SW region, just outside the virial core ($\sim 1^\circ$). In this paper we discuss measurements of line-strength indices for 74 early-type galaxies (out of which 36 are dE/dS0) in the center of the Coma cluster, while the subsequent papers will also address a region outside the cluster virial core. We provided a full description of the sample selection and spectroscopic observations in Paper I. Here, we only present a summary of our observations.

For the dE/dS0 sample selection we utilized photometry from WIYN’s Mini-Mosaic imager and the Isaac Newton Telescope Wide Field Camera. We determined the following cutoffs from color-magnitude and color-color diagrams: $0.2 < (U - B) < 0.6$ mag, $1.3 < (B - R) < 1.5$ mag and $M_B \geq -17.3$ mag (Ferguson & Binggeli 1994) assuming a distance modulus for the Coma cluster of 35.078, $d = 99$ Mpc.

We obtained the follow-up spectroscopic data with the Hydra multi-fiber spectrograph on WIYN 3.5 m telescope. The instrumental resolution was $\text{FWHM} = 1.91 \text{ \AA}$ which was sampled at $\sim 0.705 \text{ \AA px}^{-1}$. We used IRAF’s ‘dohydra’ package for data reduction. The diameter of the blue cable fiber was $3.1''$ which corresponds to ~ 1.45 kpc at the distance of the Coma cluster ($d = 99$ Mpc).

In Paper I we determined that 100% of the observed galaxies in our sample (down to $m_B \approx 19.2$ mag) are consistent with being members of the Coma cluster as their recession velocities range between 4,000 and 10,000 km s^{-1} (Colless & Dunn 1996). The luminosity of the sample spans $-20.3 \lesssim M_B \lesssim -15.8$ mag while the velocity dispersions are $30 \lesssim \sigma \lesssim 260 \text{ km s}^{-1}$. All the spectra have $S/N \geq 15$ per pixel (Paper I, also see Appendix B for S/N determination).

Throughout this paper we refer to galaxies fainter than $M_B \approx -18$ and with $\sigma < 100 \text{ km s}^{-1}$ as ‘faint’, or low- σ galaxies. This group includes the 36 dE/dS0 galaxies and 6 intermediate early-type galaxies. The remaining 32 objects with $\sigma \geq 100 \text{ km s}^{-1}$ we refer to as bright, or high- σ galaxies.

In order to determine the luminosity-weighted

ages and metallicities for the early-type galaxies in the Coma cluster we measure their spectral line-strength indices and compare them with stellar population models by Thomas et al. (2003, hereafter TMB03).

3. ABSORPTION-LINE STRENGTH INDEX MEASUREMENTS

We use the Lick/IDS system of indices (originally defined by Burstein et al. 1984; Gorgas et al. 1993; Worthey et al. 1994; Trager et al. 1998) as it covers a wide range in optical absorption-lines among which are some of the most prominent features of early-type galaxies. Furthermore, the Lick/IDS system is also a basis for an extensive collection of stellar synthesis models, allowing one to derive ages and metallicities of galaxies.

We measured the line-strengths for our 74 early-type galaxies with the software REDUCEME (Cardiel 1999), task INDEX. This software allows for careful determination of uncertainties in the index measurements as it uses Monte Carlo simulations (see Appendix A for more details). We were able to measure the following Lick/IDS indices: Ca4227, G4300, Fe4383, Ca4455, Fe4531, C₂4668, H β , Fe5015, Mg₁, Mg₂, Mg_b, Fe5270, and Fe5335 (Trager et al. 1998); and their extensions to higher order Balmer lines H γ_A and H γ_F (Worthey & Ottaviani 1997). We also include the [MgFe]’ (as defined by TMB03) and $\langle \text{Fe} \rangle$ (González 1993) indices since they closely measure metallicity and are common in the literature allowing for an easy comparison. We use these two indices with stellar population models to predict luminosity weighted ages, metallicities and the $[\alpha/\text{Fe}]$ -ratios.

The standard procedure for matching the Lick system of line-strength indices is to re-sample the data to the resolution of Lick/IDS and to correct for the systematic differences between the indices of standard stars which were also observed by Lick. Additionally, one needs to correct the nebular emission and apply velocity dispersion and aperture corrections. We were not able to fully transform our data into the Lick/IDS system because we did not observe stars in common with the original stellar library (see below). Below, we describe the procedure we followed:

i) Re-sampling to Lick/IDS resolution

We adjusted the spectral resolution of our data to match the resolution of the Lick/IDS $\sim 7-10 \text{ \AA}$ (FWHM) depending on the wavelength. This was done by broadening each galaxy spectrum by the quadratic difference between the Lick resolution and that of the observed galaxy.

$$\sigma_{broad} = \sqrt{\sigma_{Lick}^2 - \sigma_{gal}^2 - \sigma_{Instr}^2} \quad (1)$$

where σ_{broad} is the amount to broaden the galaxy by (in km s^{-1}), σ_{Lick} is Lick/IDS resolution for a particular index (see Table 5 of Sánchez-Blázquez et al. 2006a), σ_{gal} the velocity dispersion of the galaxy and σ_{Instr} represents the instrumental resolution of our data. Note that $\sigma_{obs}^2 = \sigma_{gal}^2 + \sigma_{Instr}^2$.

ii) Flux calibration

Since we lacked observations of flux calibration stars in our sample, we used the flux calibration of Sánchez-Blázquez et al. (2006a) who have 8 galaxies in common with our sample. First, we obtained the response curves for the 8 matching galaxies by dividing each galaxy spectrum by that of the flux-calibrated galaxy. Then, we fitted a polynomial function to each of the response curves and created a mean flux calibration curve. This curve is used to flux calibrate the line-strengths, while the individual response curves are later used to calculate the flux related uncertainties in the index measurements (see Appendix A).

iii) Offsets to Lick/IDS standards

We did not observe stars in common with Lick/IDS. Furthermore, we only have 4 galaxies also observed by Lick/IDS (Trager et al. 1998) which is insufficient for determining any offsets between our data and the Lick/IDS system. We are, however, able to compare our data to other data sets in the literature (see Section 4).

iv) Velocity dispersion corrections

The velocity dispersion measurements of our sample of Coma cluster galaxies are described in Paper I. The velocity dispersion corrections are usually done by, first, broadening an individual galaxy spectrum to an

effective resolution of $\sqrt{(\sigma_{Lick}^2 + \sigma_{gal}^2)}$. Second, the index measurements are corrected for the extra broadening due to velocity dispersion of the galaxy (σ_{gal}) via polynomial fitting. In our case, $\sigma_{gal} < \sigma_{Lick}$ for all but 4 galaxies in our sample. Therefore, we are able to apply the velocity dispersion corrections by broadening our spectra by $\sqrt{(\sigma_{Lick}^2 - \sigma_{gal}^2)}$ and then measuring the indices. This approach also avoids introducing a source of uncertainty associated with velocity dispersion corrections which may affect the derived $I-\sigma$ relations (Kelson et al. 2006).

v) Aperture corrections

The galaxies in our sample are typically smaller than the $3''$ aperture of HYDRA fibers (Graham & Guzmán 2003). Therefore, we found no need for aperture corrections. In fact, for most of our data, we are sampling the entire galaxy, rather than only its central parts. Since dE galaxies have flat velocity dispersion gradients (e.g. Pedraz et al. 1998), there should not be a significant change between the central and global measurements of these galaxies. Although we do not apply aperture corrections, we do recognize that a few massive galaxies in this sample are likely to be larger than the HYDRA-spectrograph fibers in which case we are sampling their central regions only.

vi) Emission corrections

It is well known that some early-type galaxies have nebular emission which can contaminate measurements of certain line-strength indices. For example, nebular emission in the $H\beta$ feature would cause the $H\beta$ line-strength index to appear lesser in value which in turn would lead to derivation of an older age for a given galaxy. We selected our sample via color-magnitude and color-color diagrams to minimize the presence of emission. We also checked the spectra for weak emission lines by: co-adding all the galaxies to enhance the S/N of any weak emission, and dividing each galaxy by its template (Kuntschner et al. 2001). Finally, we used a method similar to that of Hammer et al.

(2001) and Kuntschner et al. (2002) to determine whether any galaxies in our sample contained emission. From each galaxy spectrum we subtracted its optimal template (a spectrum of a linear combination of template stars optimized to fit each galaxy spectrum, see Paper I for more details). This method revealed that 2 galaxies in our sample had $H\beta$ and OIII emission. We exclude these two galaxies, GMP 3733 and GMP 2516, from our analysis. We note that the low number of dE/dS0 galaxies with emission is consistent with other studies in the Coma cluster (Sánchez-Blázquez et al. 2006a; Smith et al. 2008) and with dwarf galaxies having their gas removed when they enter the cluster environment.

A sample of our measurements is presented in Tables 1 and 2, while the full data set is in electronic format. These indices are at the Lick/IDS resolution, so they can be easily compared to other sources in the literature. The error in each index measurement includes uncertainties associated to the flux calibration and to the photon noise. For a more detailed description of the uncertainty measurements, please see Appendix A.

4. COMPARISON WITH LITERATURE

Converting our data to the Lick/IDS system resolution allows a direct comparison to other data sets in the literature. We compare our line strength measurements to that of Poggianti et al. (2001a, hereafter P01), (Nelán et al. 2005, hereafter NFPS) and (Smith et al. 2008, hereafter S08). Although these studies contain a significantly larger number of galaxies, our data is complementary to these samples as it includes a larger number of low mass galaxies ($\sigma \lesssim 100 \text{ km s}^{-1}$) with velocity dispersion measurements reaching as low as $\sigma \approx 30 \text{ km s}^{-1}$ in Coma.

The comparison between the three literature samples and our data are shown in Figures 1, 2, and 3. The offsets are presented in Table 3. The mean offsets are defined as a difference between the index measurement in this paper and the index measurement in P01, S08, or NFPS ($N05$) $\langle \Delta I \rangle = I_{\text{here}} - I_{\text{other}}$. We also calculated the error in the mean offset, standard deviation, and the standard deviation expected by the errors.

The offsets between our sample and S08 are small and not significant for the majority of the indices. The indices for which the offsets are significant are Mg_1 , Mg_2 and Fe5270 with mean offsets of -0.014 ± 0.003 , -0.018 ± 0.004 and -0.334 ± 0.127 , respectively. However, the scatter between the S08 sample and ours is large and cannot be explained by the errors. The indices Ca4227, G4300, $H\gamma_A$, $H\gamma_F$, and Ca4455 each have a scatter ~ 3 times larger than the scatter expected by the errors, while the scatter is ~ 2 times larger than the scatter due to the errors for majority of the other indices. The large scatter in the comparison between the S08 index measurements and ours is dominated by a group of galaxies which are systematically offset in the $H\beta$ plot (red open circles in Figure 1). Because our $H\beta$ and $[MgFe]'$ indices for these galaxies cannot be reproduced by the stellar population models, we exclude them from further analysis and revisit this issue in § 6.1. However, once these galaxies are excluded from the analysis, we no longer have a statistically significant number of galaxies in common with S08 sample for comparison.

We find that the mean offsets between our index measurements and those of Poggianti et al. (2001a) are small and in most cases insignificant. However, Ca4455, Fe5015, and Mg_1 have non-negligible offsets, -0.259 ± 0.116 , -0.652 ± 0.208 and -0.012 ± 0.006 , respectively. We note that some indices may be offset because our indices are not fully transformed to the Lick/IDS system like the P01 sample. Similarly to the S08 data, the scatter in the indices when comparing our data with P01 is large for most indices, except for Mg_1 and Mg_2 . Furthermore, the large scatter between these two data sets cannot be explained by the errors. The discrepancy between the measured scatter and the scatter due to the errors is the largest for G4300, $H\gamma_A$, $H\gamma_F$, and Mg_1 .

On the other hand, the NFPS index measurements are in good agreement with ours. Among the atomic indices only Ca4227, Fe4531 and Fe5015 have significant offsets: -0.207 ± 0.047 , -0.152 ± 0.066 and -0.313 ± 0.102 , respectively, while the rest of the indices are consistent between the two studies with a small scatter. Most noticeably, our and the NFPS indices are in very good agreement in the Mg-indices after a systematic offset in Mg_1 of -0.023 ± 0.002 and in Mg_2

of -0.017 ± 0.002 is applied. The NFPS data are not flux calibrated which would mostly affect the molecular indices like the Mg_1 and Mg_2 and may explain why there is an offset between the data sets for these two indices. However, the scatter in these two molecular indices is remarkably small (0.01 mag for both). The scatter in the remaining indices is also consistent within the errors in both studies.

We have demonstrated that our index measurements are in good agreement with those of NFPS, which is one of the highest quality data available in the Coma cluster so far. Considering our internal and external error analysis, we conclude that our data set has a similar enough quality and our error measurements are well estimated. In the following sections we only include the NFPS data set for comparison purposes, since this sample also includes velocity dispersions. The NFPS spectra were not flux calibrated, and for further analysis we apply an offset to the NFPS data to be consistent with ours according to the average values listed in Table 3.

5. INDEX – VELOCITY DISPERSION RELATIONS

In the following paragraphs we investigate the relationships between different line-strength indices and velocity dispersion (σ). We compare these relations between the low- and high- σ galaxy samples, and discuss possible parameters that drive the index- σ relations (hereafter $I - \sigma$).

5.1. Results of $I - \sigma$ Relations

We examine relations between 15 Lick/IDS indices, plus $\langle Fe \rangle$ and $[MgFe]'$, and the central velocity dispersion of our galaxies in Figure 4. In this plot, we include galaxies from our sample and galaxies in the Coma cluster from NFPS. Objects in common have averaged index values and velocity dispersions. We combined the two data sets and binned index measurements for galaxies of similar velocity dispersion. All the bins have the same narrow interval in $\log \sigma$ of 0.118 dex. The red diamonds represent the average value of each bin weighted by the uncertainties in the index measurements.

Two different types of behaviors emerge between the indices and velocity dispersions for these

early-type galaxies in the Coma cluster (Figure 4). One group of indices shows evidence for a break in the slope $\sim 100 \text{ km s}^{-1}$, **group I**, while another group exhibits strong linear relations with $\log \sigma$, **group II**. We further divide group I into 2 sub-groups where the evidence for a break in the slope is stronger for group Ia than it is for group Ib.

We plot these groups in the different columns of Figure 4. To more easily describe the difference between the groups of $I - \sigma$ trends, the plots also include separate linear fits to low- and high- σ galaxies (Table 4), even though the correlation coefficients for these fits are low for group I. This figure also contains 13 low- σ galaxies, marked as yellow filled circles, which lie outside the model grids and have been excluded from the analysis (discussed in § 6.1). We refer to these objects as “off-grid” galaxies.

Group I: Galaxies with $\sigma \geq 100 \text{ km s}^{-1}$ exhibit flat $I - \sigma$ relations in group I. On the other hand, these relations show evidence for a break in their slope for the low- σ galaxies. This break is more evident for indices in group Ia than in Ib. Both sub-groups show a significantly larger scatter of index values in the low- σ regime than for the high- σ galaxies. In Table 5, we calculated the standard deviation of the low- and high- σ galaxies for group Ia (also shown in Figure 4). The scatter of index values is ~ 2 times larger for the low- σ galaxies than it is for the high- σ ones. Additionally, the mean value of an index differs for low- and high- σ galaxies by 7–27 % for this sub-group. We also performed the Kolmogorov-Smirnov test (KS) to determine whether the two groups of galaxies come from the same distribution. In the same table, we show the KS probability that the two sets are drawn from the same distribution. Since the values of the KS probability are quite small, we conclude that low- and high- σ galaxies may indeed come from different populations. We also show the linear fits for this sub-group, although their Spearman Rank correlation coefficients (see Table 4) are small and these relations are not statistically significant.

The middle panel of Figure 4 shows the Ib sub-group of $I - \sigma$ relations, which also exhibits evidence for the break in the slope around $\sim 100 \text{ km s}^{-1}$. However, the break is not as obvious as it is for group Ia since there are a number of

low- σ galaxies whose index values are equal or higher than the high- σ galaxies. For this reason we perform linear fits for the entire σ range together. We take into account both the errors in the index and σ and calculate the intrinsic scatter (σ_{Intr}) and the scatter predicted by the errors (σ_{Err}) for both low- and high- σ galaxies (Table 6). The Spearman Rank correlation coefficients, ρ , are low (lower than 0.5) for this sub-group indicating weak or null $I - \sigma$ correlations, especially for Ca4227. Galaxies with $\sigma < 100 \text{ km s}^{-1}$ have a larger intrinsic scatter¹ than their more massive counterparts except for Ca4227 and $\langle \text{Fe} \rangle$ indices (see lower right-hand corner of Figure 4). However, the larger intrinsic scatter for high- σ galaxies in the Ca4227 index is dominated by galaxies from the NFPS data. Ca4227 is the only index for which the intrinsic scatter is smaller than the scatter due to the errors for both low- and high- σ galaxies. The remaining indices in group Ib display a larger intrinsic scatter than the scatter due to errors ($\sim 1.2 - 2.9$ times) for both low- and high- σ sub-samples, except for Fe5015 for which the intrinsic scatter is zero. The KS test on the residuals between the indices and their respective linear fits implies that only Fe5335 and $\langle \text{Fe} \rangle$ show a high enough probability that the low- and high- σ galaxies are drawn from the same population.

Group II: In the third column of Figure 4 we show the metallic indices which display a tight relation with σ . This is quantified in Table 7, where we calculated the Spearman-Rank correlation coefficients, and we include the slopes and intercepts of linear fits to these relations. We show the intrinsic scatter and the scatter expected by the errors in the bottom right hand corner of Figure 4 for each of these indices. For all indices in this group the intrinsic scatter is larger than the scatter due to errors, although the two are very close in value for Mg₁ and Mg₂. Moreover, the correlation coefficients for all the indices in this group imply a robust relation with σ . Many studies find that the early-type galaxies in clusters show a tight re-

lation between line-strength index Mg₂ and their central velocity dispersion and find similar slopes for this relation. Our slope is consistent with that of NFPS within 1 standard deviation (Table 7).

Balmer Lines: The Balmer lines H γ_A , H γ_F and H β exhibit negative slopes in their $I - \sigma$ relations. Their Spearman Rank correlation coefficients imply a strong relation for H γ_F , while the relations for H γ_A and H β have slightly lower coefficients, $\rho = -0.665$ and -0.502 respectively (Table 7). In case of H β , we see a hint for an asymmetric scatter for low- σ galaxies where more galaxies have a lower H β index. Together, our and the NFPS sample have a standard deviation from the linear fit of 0.306 with 23 galaxies having a lower value of their H β index, compared to the scatter of 0.243 for 18 galaxies with a higher H β index. The calculations exclude the galaxies which lie off the model grids.

5.2. Discussion of Index- σ relations

Historically, most studies have concentrated on relations between Mg₂, a metallicity indicator, and H β , an age indicator, with $\log \sigma$, a measure of mass, (to name a few: Terlevich et al. 1981; Dressler 1984; Guzman et al. 1992; Bender et al. 1993; Jorgensen et al. 1996; Kuntschner et al. 2001). Recent studies, however, show that these relations are more complex than originally thought. For instance, Mg₂ - σ may be significantly dependent on both age ($\sim 15\%$) and relative abundances of heavy elements ($\sim 20 - 30\%$) (Mehlert et al. 2003; Thomas et al. 2005). While H β - σ mainly depends on age, it also changes with metallicity and chemical composition (Sánchez-Blázquez et al. 2006a).

In this study we present, for the first time, the Mg₂ - σ , H β - σ and relations between other Lick indices with σ down to 30 km s^{-1} for a homogeneous sample of early-type galaxies. Our galaxies reside in one of the densest environments in the nearby universe: the center of the Coma cluster. We show that the Mg₂ - σ relation spans the entire range of $30 - 260 \text{ km s}^{-1}$ with a small scatter. We also investigate relations between the H β , H γ and the metallicity sensitive line strengths with σ . We discuss the H β - σ and Mg₂ - σ individually, while we examine the remaining indices together.

¹
$$\sigma_{Intr}^2 = \frac{\sum_{i=1}^n (\text{Index}_i - (a + b \cdot \sigma_i))^2}{N - 2} - \frac{\sum_{i=1}^n \delta_{\text{Index}_i}^2 + b^2 \cdot \delta_{\sigma_i}^2}{N}$$

where a is the intercept and b is the slope.

5.2.1. $H\beta$ vs. σ

Most studies find that the line-strength $H\beta$ and the central velocity dispersion of early-type galaxies are anti-correlated. This relation seems to hold in different environments (e.g. Fisher, Franx, & Illingworth 1995; Jorgensen 1997; Trager et al. 1998; Kuntschner 2000; Caldwell, Rose, & Concannon 2003; Nelan et al. 2005; Sánchez-Blázquez et al. 2006a) and is usually interpreted as an interplay between age and mass. However, recent evidence that the $H\beta - \sigma$ relation is weak or flat in the Coma cluster (Mehlert et al. 2003; Sánchez-Blázquez et al. 2006a) may allude towards its dependence on the environment. Furthermore, there is some evidence that the age variation of galaxies in clusters is not large and the $H\beta - \sigma$ relation may mostly be driven by metallicity Kuntschner & Davies (in Fornax 1998), or by both variations in global metallicity and relative abundance of different heavy elements for the galaxies in the Coma cluster (Sánchez-Blázquez et al. 2006a).

We confirm that the early-type galaxies in the core of the Coma cluster show a weak anti-correlation between their $H\beta$ line strength and velocity dispersions. Furthermore, we find a hint towards an asymmetric scatter for the low- σ galaxies where more galaxies have higher Balmer line-strengths (see last part of Section 5). Similarly, Caldwell et al. (2003, hereafter CRC03) also find a large asymmetric scatter for the low- σ galaxies, although in the opposite direction. It is possible that this effect is environmental, since CRC03 sample includes galaxies in lower density environments (Virgo, the field, and lower density environments) than ours. In either case, we extend the $H\beta - \sigma$ relation to low- σ galaxies down to 30 km s^{-1} in σ , or by 0.2 dex when compared to CRC03. We confirm that $H\beta$ and σ are anti-correlated, and we find a hint of an asymmetric scatter in the low- σ regime.

5.2.2. Mg_2 vs. σ

Perhaps the most studied $I - \sigma$ relation is the one of magnesium, in particular, the Mg_2 index (just to name a few studies: Terlevich et al. 1981; Gorgas, Efstathiou, & Aragon Salamanca 1990; Guzman et al. 1992; Bender, Burstein, & Faber 1993; Bernardi et al. 1998; Colless et al. 1999;

Jørgensen 1999; Concannon, Rose, & Caldwell 2000; Kuntschner 2000; Poggianti et al. 2001a; Proctor & Sansom 2002; Worthey & Collobert 2003; Mehlert et al. 2003; Sánchez-Blázquez et al. 2006a). The tight relation between Mg_2 and σ has been interpreted as evidence that all elliptical galaxies have a low dispersion in age (Bender et al. 1993; Bernardi et al. 1998). Furthermore, the parameter driving this relation has been under much debate. Originally, studies argued that the $Mg_2 - \sigma$ relation depended mostly on metallicity (Forbes et al. 1998; Terlevich et al. 1999), while age and relative abundances of different heavy elements have recently been proposed to also influence this relation (Trager et al. 1998; Jørgensen 1999; Trager et al. 2000a; Kuntschner et al. 2001; Poggianti et al. 2001b; Mehlert et al. 2003; Caldwell, Rose, & Concannon 2003; Thomas et al. 2005; Sánchez-Blázquez et al. 2006a).

Our $Mg_2 - \sigma$ relation is consistent with other studies in both the slope (Table 7) and the low intrinsic scatter. Although, we note a slightly larger dispersion around the line for low- σ galaxies, for the first time, we confirm that this relation is robust for the entire range ($30\text{--}250 \text{ km s}^{-1}$) in σ .

5.2.3. $I - \sigma$ trends in general

A surprising result in this paper are the different shapes of $I - \sigma$ relations once we include galaxies with $\sigma < 100 \text{ km s}^{-1}$. Most studies find linear $I - \sigma$ relations for early-type galaxies. However, these samples are limited to galaxies with $\sigma \gtrsim 50 \text{ km s}^{-1}$. Although our Coma cluster data is not larger than most other studies, it is unique as our sample contains ~ 40 galaxies with $30 \leq \sigma < 100 \text{ km s}^{-1}$ (see Paper I).

We find that for the majority of indices, the low- σ galaxies exhibit a larger scatter in the $I - \sigma$ relations than the high- σ galaxies. Concannon, Rose, & Caldwell (2000) also found that the scatter in index- σ relations is larger for low mass galaxies. Their interpretation of this result for the $H\beta - \sigma$ relation is that the low mass galaxies have experienced a more varied star formation history and have a larger spread in age. Similarly, Sánchez-Blázquez et al. (2006a) show that the scatter in the $I - \sigma$ relations is mainly a consequence of the element abundances varying with age. We investigated whether the shapes of the $I - \sigma$ relations are related to the

variations in individual element abundances using Tripicco & Bell (1995), Thomas et al. (2003) and Korn et al. (2005).

Indices in the left column (group Ia) of Figure 4 have strong Fe-dependence in common, except for Fe4531 and G4300 which mostly depend on Ti and to a lesser extent on Fe. Group Ib contains indices which depend on both, α -peak elements and Fe. In group II we again find a mixture of elements driving the indices. Carbon and α -peak elements, Mg and O in particular, do appear to influence most indices in this column, with the exception of $[\text{Mg/Fe}]'$ which does not depend much on the $[\alpha/\text{Fe}]$ ratio (Thomas, Maraston, & Bender 2003). Finally, $\text{H}\gamma_{A,F}$ indices depend on the $[\alpha/\text{Fe}]$ ratio although this dependency diminishes with increasing metallicity (Korn et al. 2005), while the $\text{H}\beta$ index is moderately influenced by elemental abundance ratios. If the abundance ratios are what drives the relation between the higher order Balmer lines and σ , then there is a possibility that the larger scatter of these indices toward the low- σ galaxies is caused by the decreased metallicity. In conclusion, we do not find any clear correlations between the shape of the $I-\sigma$ relations with the element abundance driving the indices, neither with α - nor Fe-peak elements.

Poggianti et al. (2001a) find that the slopes of the index-magnitude relations can be explained by trends between the age and metallicity with luminosity. These relations are an alternate form of the $I-\sigma$ relations, since magnitude and σ are related via the Faber-Jackson relation. Sánchez-Blázquez et al. (2006a) find that variations in these two parameters are not sufficient to explain the $I-\sigma$ slopes. They conclude that a likely explanation for the different $I-\sigma$ relations could be the relative abundance of elements $[\text{Mg/Fe}]$, $[\text{C/Fe}]$, and $[\text{N/Fe}]$, as already speculated by other authors (Worthey, Faber, & Gonzalez 1992; Greggio 1997; Jorgensen 1997; Kuntschner 2000; Trager et al. 2000a; Thomas, Maraston, & Bender 2002; Mehlert et al. 2003; Thomas et al. 2005). More specifically, Sánchez-Blázquez et al. (2006a) show that the $I-\sigma$ slopes are best reproduced when the α -peak elements change more than the Fe-peak elements and, the $[\text{Mg/Fe}]$ and $[\text{N/Fe}]$ ratios change more than the rest of the alpha elements with σ . We find no clear evidence in support of these results.

The answer to the different shapes of $I-\sigma$ relations may lie in the finding that C_24668 , Mg_1 , Mg_2 and Mg_b , **all** in group II (exhibiting robust linear relations), are independent of the micro-turbulent velocity of stellar atmospheres (Tripicco & Bell 1995). This is unusual, since most other indices depend on this parameter. In fact, according to Tripicco & Bell (1995), changing the micro-turbulent velocity of stellar atmospheres just by 1 km s^{-1} causes changes in the indices which are more significant than if one were to double the metal abundance. Hence, the shape and/or tightness of the $I-\sigma$ relations for metallic lines may be determined by how much an index depends on the micro-turbulent velocity of the underlying stellar atmospheres.

6. AGES, METALLICITIES AND ELEMENT ABUNDANCES OF EARLY-TYPE GALAXIES

One of the main goals of this paper is to derive ages and metallicities of faint early-type galaxies in the central region of the Coma cluster. This is possible through evolutionary stellar synthesis models. We use index-index diagrams to compare the observed line-strengths with the stellar population models (SPM) of Thomas, Maraston, & Korn (2004, hereafter TMK04), an extension of TMB03, to derive the ages, metallicities and abundance ratios for our sample of galaxies.

The models that we use are based on the evolutionary population synthesis code from Maraston (1998). They account for element ratio changes based on the response functions from Korn et al. (2005) via a method similar to the one introduced by Trager et al. (2000b). The TMB03 models span a range in age between 1 and 15 Gyr, total metallicity, $[\text{Z/H}]$, from -2.25 to 0.65 , and the α -ratio values of $0.0-0.5$. Using an age-sensitive index vs. a metallicity-sensitive index with the models allows for a derivation of ages, metallicities and α -ratios of galaxies.

We use $\text{H}\beta$ as the main indicator of age. This line-strength is only marginally sensitive to the α/Fe ratio, while the higher order Balmer lines are significantly affected by $[\alpha/\text{Fe}]$ at super-solar metallicities (TMK04). Furthermore, $\text{H}\beta$ is a prominent feature in the spectra of our galaxies.

As a metallicity gauge we use the $[\text{MgFe}]'$ index as defined by TMB03, albeit it is also dependent on age. This index is sensitive to the overall metallicity and, similarly to $\text{H}\beta$, depends little on the $[\alpha/\text{Fe}]$ ratio.

We use a combination of the $\text{H}\beta$ - $[\text{MgFe}]'$, and $\langle\text{Fe}\rangle$ - Mg_b indices to determine the ages, metallicities and the α -ratios for our Coma galaxies. However, before investigating the relations between age, metallicity and $[\alpha/\text{Fe}]$ we note that, due to the tilt of the model grids and the given errors in individual indices, the errors in derived ages and metallicities are likely to be correlated (Kuntschner et al. 2001; Terlevich & Forbes 2002). In order to reduce the error in the line-strength indices (and therefore the correlated errors in the derived parameters) we have obtained an average value of each index for galaxies with similar velocity dispersions (for σ bins, see Table 8). These average values binned by velocity dispersion represent “average” or “binned” galaxies.

As a precursory step, we plot our galaxies on top of the model grids in Figure 5. In the left panel of this figure, we fixed the α -ratio to the solar value according to the findings of Gorgas et al. (1997), so that we can determine the ages and metallicities. While in the $\langle\text{Fe}\rangle$ - Mg_b panel, the age is set to 6 Gyr, as this is an average age of our low- σ galaxies and corresponds to the ages derived from our paper I. Once the age is at a fixed value, we can determine the metallicities and the $[\alpha/\text{Fe}]$. We marked the low- and high- σ galaxies with different symbols and also included the “average galaxies” for which the indices are binned by velocity dispersion.

The Coma cluster galaxies in our sample exhibit a wide range in both their ages and metallicities. Further, the more massive galaxies have, on average, metallicities equal to or larger than solar, while the low- σ galaxies (the three smallest diamonds) have on average, subsolar metallicities and younger ages. Similar results of wide age and metallicity ranges have already been noted by other authors in the literature for both the Coma cluster (Jørgensen 1999; Poggianti et al. 2001a; Mehlert et al. 2003; Nelan et al. 2005; Sánchez-Blázquez et al. 2006b), and for the lower density environments (Caldwell et al. 1993; Jørgensen 1997; Trager et al. 1998, 2000b; Nelan et al. 2005; Sánchez-Blázquez et al. 2006b; Bernardi et al.

2006).

Our sample seems to split around $[\text{MgFe}]' \sim 3$, or more precisely around the solar metallicity. This is in agreement with Poggianti et al. (2001a) who find that their faint Coma cluster galaxies are divided into two groups, one being metal-rich and the other one metal-poor. In our sample, galaxies with the super-solar metallicities are predominantly high- σ early-types. A group of low- σ galaxies is also present in this regime and these galaxies are on average younger than the high- σ galaxies. In contrast, all the other low- σ galaxies exhibit sub-solar metallicities. This result may imply two different formation mechanisms for low- σ early-type galaxies within the Coma cluster. Alternatively, galaxies entering the cluster environment at different epochs would be stripped from their gas at different evolutionary stages, possibly explaining the metallicity differences. An investigation of these parameters and their dependence on the position within the cluster and the cluster environment is a topic of our future papers.

On the other hand, Mehlert et al. (2003) and Thomas et al. (2005) find that their samples of early-type galaxies split into two subclasses at $\text{H}\beta \sim 2 \text{ \AA}$ where the younger subclass has solar or higher metallicities on the $\text{H}\beta$ - $[\text{MgFe}]'$ plot. Mehlert et al. (2003) find that the ‘young clump’ (their Figure 4) is dominated by S0 galaxies, rather than Es. Thomas et al. (2005) attribute this division to either younger stellar populations or blue horizontal branch stars. Here too, we can argue that such a division exists for the low- σ galaxies in our sample, but not for the more massive Es. We denote a group of galaxies with old ages and low metallicities, while the remaining low- σ galaxies in our sample have intermediate ages and a large range in metallicity. This suggests that some low mass early-type galaxies harbor younger stellar populations, while the others are old and metal poor. We also found no correlation with morphology for this result.

The right panel of Figure 5 shows a relation of the Mg_b and $\langle\text{Fe}\rangle$ indices overlaid with models. When the age is fixed, it is possible to derive the $[\alpha/\text{Fe}]$ ratios for these galaxies. Similar to the $[\text{MgFe}]'$ vs. $\text{H}\beta$ plot, there is a division in the sample between galaxies around the solar metallicity in this figure. Majority of galaxies with super-solar metallicities are high- σ galax-

ies. They cluster around $[\alpha/\text{Fe}] = 0.3$ which is consistent with the well-known overabundance of Mg among Es, i.e., a depression of Fe with respect to the solar values (Trager et al. 2000a). Although the low- σ galaxies show a wider range in α -ratios (0.0–0.5) than their more massive counterparts, the majority of low- σ galaxies, with the exception of a few objects, have low $[\alpha/\text{Fe}] \lesssim 0.2$. This result indicates that the low-mass galaxies have had a more extended star formation history (Gorgas et al. 1997)

6.1. Off-Grid Galaxies

Our sample contains 13 dE/dS0 galaxies that are not fitted by the models when using $\text{H}\beta$ – $[\text{MgFe}]'$ indices (bottom left corner of Figure 5). To see whether we can recover their ages, we plot $\text{H}\gamma_A$ and $\text{H}\gamma_F$ with $[\text{MgFe}]'$ in Figure 6. Even when we use a different Balmer line strength, $\text{H}\gamma$, 8 out of 13 galaxies still lie off the model grids. All of these galaxies are low mass with $30 \leq \sigma < 70 \text{ km s}^{-1}$. In the following paragraphs we perform a number of tests to determine whether these galaxies truly have such low values of the $\text{H}\beta$ index.

First, we checked for a possibility of nebular emission in the $\text{H}\beta$ feature, as it would make this line strength appear weaker, i.e. yielding older ages. Aside from the test that we have already performed by dividing each spectra with its optimal template (see § 3), we also stacked the spectra of these galaxies together (since they have a small range in σ) at the original resolution (FWHM = 1.9 Å) and checked for any possible emission in the $\text{H}\beta$ absorption feature (Figure 7) which was not detected previously. At this resolution, we do not find any contamination of the off-grid galaxies by nebular emission.

Second, we considered possible sky subtraction and scattered light problems. If scattered light was the cause of the low $\text{H}\beta$ index values, not only $\text{H}\beta$ but the rest of the indices should be affected as well. Further, wrongly subtracted sky levels should also lead to asymmetrical residuals at the locations of the bright sky lines. However, this was not the case in our spectra, and we exclude sky subtraction and the scattered light correction as causes of the low $\text{H}\beta$ index values.

Third, we checked whether these off-grid galaxies were consistent with the position of globular

clusters (hereafter GCs) on the $[\text{MgFe}]'$ vs. $\text{H}\beta$ plot. If the models would extend to these galaxies, they would correspond to very old and very metal-poor objects similar to GCs or they could also be “primordial” as suggested by Rakos & Schombert (2004). Figure 5 shows a possibility that some of the off-grid galaxies are consistent with GCs, while a number of these galaxies lie in a region even older and more metal poor than GC.

We also checked whether the $\text{H}\beta/\text{H}\gamma_{A,F}$ ratios for the off-grid galaxies are consistent with the other galaxies in our sample and with GCs from Cenarro et al. (2007). This is shown in Figure 8. The off-grid galaxies deviate noticeably from the $\text{H}\gamma_A$ and $\text{H}\gamma_F$ with $\text{H}\beta$ plots when compared to other Coma galaxies in our sample and the GCs. Interestingly, the off-grid galaxies show no deviations in the $[\text{Mg}/\text{Fe}]$ plot. This points toward a possibility of some problems in the measurements of the Balmer lines for these off-grid galaxies, which is not necessarily true for the other indices.

Finally, we were able to compare our spectra with those of S08 (also private communication with Russell Smith). The comparison showed that the spectra of the off-grid galaxies likely suffered from some spurious high-resolution frequency patterns found only in the Balmer continuum bands used to measure the index. However, this is not the case for the rest of our galaxies which have good quality. To err on the safe side we exclude these galaxies from the analysis in this paper.

6.2. Method of Deriving SPM Parameters

We use an iterative procedure similar to Thomas et al. (2005) to derive the ages, metallicities and α -ratios for our sample of early-type galaxies in the Coma cluster. This procedure consists of, first, determining the age and metallicity of each galaxy by interpolating the model grids for the $[\text{MgFe}]'$ – $\text{H}\beta$ plot, at a given α -ratio. This particular combination of indices has low sensitivity to abundance ratios and is, therefore well suited for determining the other two SPM parameters, age and metallicity. Then, we fix the age as it was derived in the first step, and we derive the $[\alpha/\text{Fe}]$ and metallicity with $\langle\text{Fe}\rangle$ – Mg_b index combination. This two-step procedure is repeated until the metallicities derived from $[\text{MgFe}]'$ – $\text{H}\beta$ and $\langle\text{Fe}\rangle$ – Mg_b match well (i.e. better than 15%

difference).

We used the same iterative procedure for deriving the error ellipse in age, metallicity and α -ratio values for each galaxy. We treated the extremes of the index uncertainties as individual values. Conservatively, we chose the highest value of the error ellipse for the uncertainty in the SPM parameter. The ages, metallicities and α -ratios together with their respective errors are shown in Tables 1 and 2, while these parameters for the binned galaxies are in Table 8.

Our data of early-type Coma galaxies span a wide range in all SPM parameters. The low- σ galaxies have on average: lower ages, 6.1 ± 0.1 vs. 8.9 ± 0.1 Gyr for high- σ galaxies; lower metallicities, -0.050 ± 0.003 vs. 1.131 ± 0.004 dex; and slightly lower $[\alpha/\text{Fe}]$, 0.173 ± 0.002 vs. 0.238 ± 0.002 , closer to the solar value of 0.0. Here, we excluded the galaxies which lie off the model grids as discussed in § 6.1.

7. MODEL PARAMETERS VS. σ

In the index-index figures overlaid with models and mentioned in the previous section, we notice a trend with mass for our galaxies. Henceforth, we plot the model parameters, age, metallicity and $[\alpha/\text{Fe}]$ vs. $\log \sigma$ for the 5 velocity dispersion bins, (Figure 9). We also include the individual galaxies in these plots although we perform the linear least-squares regression (see Table 9) for the binned data only. The bin values for the age, metallicity and $[\alpha/\text{Fe}]$ were calculated by averaging these parameters for individual galaxies within each bin. The errors in the model-derived average parameters were determined by taking the standard deviation of the individual parameter values within each bin and then dividing by the square root of the number of galaxies in the bin. Although not statistically significant, trends emerge between the age, metallicity and $[\alpha/\text{Fe}]$ with σ , and we compare them to the same relations from Nelan et al. (2005).²

²We excluded one galaxy from the linear regression (GMP 2585) since this galaxy is clearly an outlier in both metallicity- and $[\alpha/\text{Fe}]$ - σ plots and it has an unusually low metallicity and a high value of $[\alpha/\text{Fe}]$.

7.1. Age- σ

The top panel of Figure 9 shows the relation between \log age and $\log \sigma$. The linear fit between these two parameters is uncertain due to the large errors in age. However, both the binned and the individual galaxies in this figure provide clear evidence for a trend between age and σ where the low- σ galaxies display younger ages.

Within the errors, our age- $\log \sigma$ trend is consistent with Nelan et al. (2005), although there are some differences. Nelan et al. (2005) find that the age- $\log \sigma$ relation steepens for the low-mass galaxies. We do not find this effect, since the age- $\log \sigma$ for these galaxies levels off at ~ 4 Gyr in our case.

Whether the age- σ relation exists for early-type galaxies or not is still an unresolved issue in the literature. Jørgensen (1999), Kuntschner et al. (2001), Mehlert et al. (2003), Thomas et al. (2005), and Sánchez-Blázquez et al. (2006b) do not find a relation between these parameters, although results from Sánchez-Blázquez et al. (2006b) yield a relation for galaxies in low density environments. However, at least a trend between age and σ is found in the samples of Concannon, Rose, & Caldwell (2000), Poggianti et al. (2001a), Caldwell, Rose, & Concannon (2003), Proctor et al. (2004), Nelan et al. (2005), and Bernardi et al. (2006). Additionally, Nelan et al. (2005) derive age- σ relations for other sources in the literature and find them to be in agreement with their data.

Although we find an age- σ trend for our sample of Coma early-type galaxies, the uncertainties in the age measurements are large and we cannot confirm a relation between these two parameters. Nonetheless, we observe that the low- σ galaxies exhibit, on average, younger ages than their more massive counterparts.

In paper I, we used the scatter in the Color- σ relation and the evolutionary stellar population synthesis models of Bruzual & Charlot (2003) to estimate the formation epoch for our Coma galaxies. We found that, if we assume a strong coordination in the formation epoch of galaxies in the Coma cluster, most of these galaxies would have formed about 6 Gyr ago and within a scatter of 1 Gyr. The results from our previous paper are consistent with those shown in the age- σ panel of Figure 9. We find that the average age of low- σ galaxies is ~ 6 Gyr and the scatter in the $\log \sigma$ - \log

age relation implies a scatter in formation epoch of ~ 1.5 Gyr.

7.2. Metallicity– σ

We also find a trend between metallicity and $\log \sigma$ (shown in the middle panel of Figure 9). The high- σ early-type galaxies tend to be more metal-rich than the low- σ galaxies which also exhibit a larger range in their metallicities.

Our derived slope, $[Z/H] \propto \sigma^{0.53 \pm 0.13}$, is in agreement with a number of studies which find a fairly robust metallicity– σ relation (Kuntschner et al. 2001; Mehlert et al. 2003; Nelan et al. 2005; Thomas et al. 2005; Sánchez-Blázquez et al. 2006b; Bernardi et al. 2006). Furthermore, our metallicity– σ trend is in good agreement with that of Nelan et al. (2005) which is also shown in Figure 9. We extend this trend to galaxies with $\sigma = 30 \text{ km s}^{-1}$ with no evidence for a change of slope or offset.

7.3. $[\alpha/\text{Fe}] - \sigma$

The $[\alpha/\text{Fe}]$ also increases with increasing σ (bottom panel in Figure 9). The low mass early-type galaxies exhibit α -ratios closer to the values in the solar neighborhood, although the trend is suggestive of $[\alpha/\text{Fe}] > 0$ even at the lowest σ . The higher mass galaxies have an overabundance of $[\alpha/\text{Fe}]$.

A relation between $[\alpha/\text{Fe}]$ and σ has already been noted by a number of authors in the literature (Trager et al. 2000b; Kuntschner et al. 2001; Proctor & Sansom 2002; Mehlert et al. 2003; Thomas et al. 2005; Bernardi et al. 2006), although conflicting with Proctor et al. (2004). In accordance to the former studies, we find that the α -ratio increases with increasing velocity dispersion. However, due to large uncertainties, we can only confirm a trend and not a correlation between these parameters.

Our $[\alpha/\text{Fe}]$ – σ slope of 0.17 ± 0.07 is shallower than the slopes derived by other authors who find ~ 0.3 (Trager et al. 2000b; Thomas et al. 2005; Nelan et al. 2005). However, we note that there are 3 objects in the $[\alpha/\text{Fe}]$ – σ plot with α -ratios that are quite large. These “outlying” points are affecting the average values of $[\alpha/\text{Fe}]$ at a given σ toward smaller values and, therefore the slope. If we were to exclude these three galaxies (GMP 2306, GMP 3855 and GMP 3780), our slope would be 0.22 ± 0.06 which is consistent with other au-

thors.

In general, super-solar α -ratios denote that galaxies formed quickly, i.e., on short star formation time-scales, and at high redshifts (Matteucci 1994). Therefore, an $[\alpha/\text{Fe}]$ – σ trend suggests that the low- σ galaxies had more extended star formation histories than their massive counterparts where new stars formed from already metal-enriched environment (Gorgas et al. 1997). In fact, a couple of mechanisms explaining the extended star formation histories of the low mass galaxies already exist. One involves UV background radiation which can extend the duration of star formation by suppressing cooling more effectively in low mass galaxies (Kawata 2001). While the other uses a combination of cooling, star formation, energy feedback, and chemical evolution to extend the star formation history of these galaxies (Chiosi & Carraro 2002).

8. TRENDS BETWEEN THE AGE, METALLICITY AND α -RATIO

In Figure 10 we investigate relations between metallicity and age, $[\alpha/\text{Fe}]$ and age, and metallicity and $[\alpha/\text{Fe}]$ for our sample of Coma cluster early-type galaxies. We do not find any relations between the model parameters for all the galaxies in our sample. However, when we examine the difference between the high- and low- σ galaxies, we find trends in the age-metallicity and the metallicity– $[\alpha/\text{Fe}]$ plots.

We do not find any correlations between age and $[\alpha/\text{Fe}]$, nor between metallicity and $[\alpha/\text{Fe}]$ even at a fixed velocity dispersion. However, we do note a weak tendency for the high- σ galaxies to have higher α -ratios and to be more metal rich than the low- σ galaxies. This effect is stronger in the Michielsen et al. (2007) sample (their Figure 7) whose data extend to lower metallicities and are in lower density environment than our Coma cluster galaxies. Assuming that our and the Michielsen et al. (2007) sample span a similar range in σ , and that the metallicity-abundance trends are not due to correlated errors, there is a possibility that this effect, too is due to the environment.

The relation between the age and metallicity at a given σ was first discussed by Trager et al. (2000a). We study the possibility of such rela-

tions for our low- and high- σ galaxies. The Spearman Rank coefficients (Table 10) imply that the relations between the age and the metallicity exist for the two σ -sub-samples, while no correlations were found for either the age- $[\alpha/\text{Fe}]$ nor the metallicity- $[\alpha/\text{Fe}]$. Note that the one galaxy, marked by a cross in Figure 10, which we excluded from the Spearman Rank test and linear regression is a galaxy with the lowest $\sigma = 30 \text{ km s}^{-1}$ in our sample.

Existence of an age-metallicity relation where galaxies with younger ages tend to be more metal rich, implies that these young galaxies have had multiple star formation episodes and that they had to form their stars from already enriched gas. This relation has been noted in numerous works both in low density environments and clusters (Trager et al. 1998; Jørgensen 1999; Kuntschner 2000; Kuntschner et al. 2001; Poggianti et al. 2001a; Terlevich & Forbes 2002; Sánchez-Blázquez et al. 2006b, to name a few). Some studies, however, suggest that this relation is a consequence of correlated errors (Trager et al. 1998, 2000a; Ferreras, Charlot, & Silk 1999; Kuntschner et al. 2001). While Poggianti et al. (2001a) observe an age-metallicity relation at all magnitudes in the Coma cluster, Sánchez-Blázquez et al. (2006b) do not find this relation in Coma and argue that their apparent trend is due to correlated errors, although they also note a possibility that their sample is biased toward high- σ galaxies, making the age-metallicity appear flat.

High- σ galaxies follow the same relation as the age-metallicity relation found by Trager et al. (2000a). To investigate this, we estimated an average correlated error for our galaxies from the error ellipse derived with the iterative process as described in § 6. The direction and size of this correlated error are shown in the top right corner of Figure 10. As it can be seen, the direction of the correlated errors coincides with the slope of the age-metallicity relation. Furthermore, the size of the errors is consistent with the extent of the distribution of age and metallicity values. This implies that the age-metallicity correlation at a given velocity dispersion may be simply the result of correlated errors in both parameters!

The linear regression between the ages and metallicities for the low- and high- σ galaxies shows that the slopes for the two sub-samples are ef-

fectively the same, but offset with different zero points. At a given age, the high- σ galaxies are more metal rich by a factor of ~ 2 than the low- σ galaxies. Similarly, at a given metallicity, the low- σ galaxies are ~ 3 Gyr younger than their more massive counterparts. This result also compares well with Michielsen et al. (2007) whose data sample contains dE galaxies from the Virgo cluster and the field. Both data sets are well anchored to the sample of massive Es from Sánchez-Blázquez et al. (2006b). However, there are differences in the distribution of galaxies between our and their sample in the age-metallicity diagram (their Figure 7). The Coma cluster galaxies exhibit a similar range of ages to the Michielsen et al. (2007) dEs, but they have a smaller range in metallicity. This points towards an environmental dependence of the age-metallicity relation since the central region of the Coma cluster is one of the densest regions in the local universe. Unfortunately, we cannot say this with certainty without knowing how low in σ the Michielsen et al. (2007) sample goes, since the one galaxy in our sample with very low metallicity on the age-metallicity plot is a galaxy with the lowest $\sigma = 30 \text{ km s}^{-1}$. The effect of finding the wider range in metallicity in the lower-density environments than in the core of the Coma cluster, thus, may be purely due to sampling galaxies with lower velocity dispersions.

9. CONCLUSIONS

In this paper we study the properties of the underlying stellar populations of faint early-type galaxies in the core of the Coma cluster. Our sample is one of the largest homogeneous samples of cluster dE/dS0 galaxies to date with velocity dispersions measurable down to $\sigma = 30 \text{ km s}^{-1}$. We present relations between 15 line strength indices with σ and extend them to the dE/dS0 galaxies. We confirm that, when we include these faint early-type galaxies, the Mg_2 relation and the $\text{H}\beta - \sigma$ anti-correlation correspond well with other sources in the literature.

We find evidence for two types of behaviors between the metallic indices and σ 's. One set of indices (C_24668 , Mg_1 , Mg_2 , Mg_b , $[\text{MgFe}]'$) exhibit tight linear relations with σ , which was also shown by other studies. The second group of $I - \sigma$ relations show a break in their slope where this break

is more evident in a sub-set including Ca4227, Fe5015, Fe5335, $\langle \text{Fe} \rangle$ than a sub-set with G4300, Fe4383, Ca4455, Fe4531 and Fe5270.

We also find that the relations between the Balmer lines and σ have negative slopes and are fairly robust, with $\text{H}\beta - \sigma$ having the weakest correlation coefficient. We find a hint of an asymmetric scatter in the $\text{H}\beta - \sigma$ relation with more galaxies having a lower $\text{H}\beta$ index. Since the asymmetry is in the opposite direction from the one found in the lower density environments (Concannon, Rose, & Caldwell 2000), it is possible that this effect depends on the environment.

Although majority of the indices are influenced by the overall metallicity, we also investigated whether each $I - \sigma$ group of indices is driven by the α - or Fe-peak elements. We found no connection between these elements and the occurrence of the break in the slope for the $I - \sigma$ trends. However, the non-Balmer indices with tight $I - \sigma$ relations are all independent of micro-turbulent velocity of stellar atmospheres. This may be a main factor which determines the shape and/or tightness of the $I - \sigma$ relations for metal-dependent line strengths.

We use the stellar population models to derive ages, metallicities and $[\alpha/\text{Fe}]$ for our Coma cluster galaxies. We find a wide range in all the SPM parameters where the galaxies with super-solar metallicities are dominated by the high- σ galaxies, while the low- σ galaxies are on average younger, have lower metallicities and their α -ratios scatter around the solar value. This implies that the low- σ galaxies had some residual star formation in their recent history, and that their star formation histories are more extended than they are for the high- σ galaxies. These results are also confirmed by the trends we find between the age, metallicity and $[\alpha/\text{Fe}]$ with σ .

We find that the age-metallicity anti-correlation is most likely due to correlated errors. We were able to compare our results with those of Michielsen et al. (2007) who observed dE galaxies in the Virgo cluster and the field. Our Coma cluster galaxies seem to have a smaller range in metallicity when compared to the Michielsen et al. (2007) data set. Therefore, there is a possibility of an environmental effect on the metallicity range for dE/dS0 galaxies, unless the Michielsen et al. (2007) data include galaxies with lower velocity

dispersions.

We thank J. Cenarro for his help on investigating the spectra for potential problems and for providing the GC data. We are also grateful to Russell Smith for providing the data from the Hectospec Coma cluster survey and double checking our measurements. R. G. gratefully acknowledges University of Yale for the awarded nights at WIYN telescope. P. Sánchez-Blázquez acknowledges the support by a Marie Curie Intra-European Fellowship within the 6th European Community Framework Programme. We also thank the anonymous referee whose suggestions have improved this work.

A. APPENDIX UNCERTAINTY MEASUREMENTS

We created the “error spectra” which allowed us to measure the uncertainties in our line-strength measurements. This process consisted of multiple steps. First, we produced an optimal template for each galaxy by combining the 6 template stars (same procedure as in Paper I). The template stars are primarily G and K spectral type and are well matched with the dominating stellar population of early-type galaxies. Then, we shifted the optimal template of each galaxy to the rest frame and broadened this spectra and that of the galaxy to the resolution of Lick/IDS. Optimal template is a spectrum of a linear combination of template stars optimized to fit each galaxy spectrum, (see Paper I for more details). We then found a polynomial fit (we chose the 7th order polynomial) to the galaxy’s and the template’s black body curve. This allowed us to calculate the residuals between the galaxy spectrum and the “model galaxy” in the following way:

$$R = G - \left(\frac{T}{P_T} \times P_G \right) \quad (\text{A1})$$

where R represents the residuals, G the galaxy spectrum, T the optimal template spectrum, P_G the polynomial fit to the galaxy spectrum, and P_T the polynomial fit to the template. The quantity in the parentheses is the “model galaxy”, a spectrum with the exact shape of the galaxy and high S/N features of the optimal template. R refers to the residual noise between the galaxy spectrum and the model galaxy.

However, to build a true error spectrum we must take into account the actual noise of the galaxy together with the uncertainty due to the template mismatch. We did this by taking the square root of the galaxy and scaling this spectrum to the average number of its counts. Then, we multiplied that quantity by the amount of noise from the residuals:

$$E = \frac{\sqrt{G}}{\langle \sqrt{G} \rangle} \times \sqrt{\langle R^2 \rangle} \quad (\text{A2})$$

Here, E is the error spectrum, $\langle \sqrt{G} \rangle$ is the average number of counts of the square root of the galaxy, and $\langle R^2 \rangle$ is the average number of counts of residuals squared. The error spectrum created in this way is, in a sense, a spectrum of the exact same shape as the galaxy with the level of noise which takes into account the Poissonian noise and the uncertainty due to the mismatch between the templates and the galaxy spectrum. Additionally, we calculate the uncertainty associated with the flux calibration. The program INDEX estimates the uncertainties associated to flux calibration by measuring the line-strength indices with all the individual response curves and computing the standard deviation from these measurements. In summary, our uncertainty measurements include the photon noise, the error due to the mismatch between the galaxy and the template, and the flux related error.

B. DETERMINING SIGNAL-TO-NOISE RATIO

In our study of both the internal kinematics and stellar populations of the faint early-type galaxies, we consider only the galaxies whose average signal-to-noise ratio $S/N \geq 15$ (see Paper I). There are 74 galaxies in our central Coma cluster sample which satisfy this condition. The S/N which we calculate for our galaxies is an average value of S/N per pixel

Determining the S/N ratio involved a couple of steps. A few of these steps are already described in § A, where we also show how one finds the residuals (Equation A1) between the galaxy spectrum and the model galaxy. We define an average value of S/N per pixel of each galaxy as:

$$S/N = \frac{\langle G \rangle}{\sqrt{\langle R^2 \rangle}} \quad (\text{B1})$$

The value of S/N ratio calculated in this way is an average value for each galaxy and it includes the mismatch between the actual galaxy spectrum and that of the model galaxy.

REFERENCES

- Bender, R., Burstein, D., & Faber, S. M. 1993, *ApJ*, 411, 153
- Bernardi, M., Nichol, R. C., Sheth, R. K., Miller, C. J., & Brinkmann, J. 2006, *AJ*, 131, 1288
- Bernardi, M., Renzini, A., da Costa, L. N., Wegner, G., Alonso, M. V., Pellegrini, P. S., Rit e, C., & Willmer, C. N. A. 1998, *ApJ*, 508, L143
- Brodie, J. P., & Huchra, J. P. 1991, *ApJ*, 379, 157
- Bruzual, G., & Charlot, S. 2003, *MNRAS*, 344, 1000
- Burstein, D., Faber, S. M., Gaskell, C. M., & Krumm, N. 1984, *ApJ*, 287, 586
- Caldwell, N. 1983, *AJ*, 88, 804
- Caldwell, N., Rose, J. A., & Concannon, K. D. 2003, *AJ*, 125, 2891
- Caldwell, N., Rose, J. A., Sharples, R. M., Ellis, R. S., & Bower, R. G. 1993, *AJ*, 106, 473
- Cardiel, N. 1999, Ph.D. thesis, Universidad Complutense de Madrid, Spain, (1999)
- Cenarro, A. J., Beasley, M. A., Strader, J., Brodie, J. P., & Forbes, D. A. 2007, *AJ*, 134, 391
- Chiosi, C., & Carraro, G. 2002, *MNRAS*, 335, 335
- Colless, M., Burstein, D., Davies, R. L., McMahon, R. K., Saglia, R. P., & Wegner, G. 1999, *MNRAS*, 303, 813
- Colless, M., & Dunn, A. M. 1996, *ApJ*, 458, 435
- Concannon, K. D., Rose, J. A., & Caldwell, N. 2000, *ApJ*, 536, L19
- Denicol o, G., Terlevich, R., Terlevich, E., Forbes, D. A., & Terlevich, A. 2005, *MNRAS*, 358, 813
- Dressler, A. 1984, *ApJ*, 281, 512
- Ferguson, H. C., & Binggeli, B. 1994, *A&A Rev.*, 6, 67
- Ferreras, I., Charlot, S., & Silk, J. 1999, *ApJ*, 521, 81
- Fisher, D., Franx, M., & Illingworth, G. 1995, *ApJ*, 448, 119
- Forbes, D. A., Ponman, T. J., & Brown, R. J. N. 1998, *ApJ*, 508, L43
- Gonz alez, J. D. J. 1993, Ph.D. thesis, AA(Univ. California, Santa Cruz.)
- Gorgas, J., Efstathiou, G., & Aragon Salamanca, A. 1990, *MNRAS*, 245, 217
- Gorgas, J., Faber, S. M., Burstein, D., Gonzalez, J. J., Courteau, S., & Prosser, C. 1993, *ApJS*, 86, 153
- Gorgas, J., Pedraz, S., Guzman, R., Cardiel, N., & Gonzalez, J. J. 1997, *ApJ*, 481, L19
- Graham, A. W., & Guzm n, R. 2003, *AJ*, 125, 2936
- Greggio, L. 1997, *MNRAS*, 285, 151
- Guzman, R., Lucey, J. R., Carter, D., & Terlevich, R. J. 1992, *MNRAS*, 257, 187
- Hammer, F., Gruel, N., Thuan, T. X., Flores, H., & Infante, L. 2001, *ApJ*, 550, 570
- Jorgensen, I. 1997, *MNRAS*, 288, 161
- J orgensen, I. 1999, *MNRAS*, 306, 607
- Jorgensen, I., Franx, M., & Kjaergaard, P. 1996, *MNRAS*, 280, 167
- Kawata, D. 2001, *ApJ*, 558, 598
- Kelson, D. D., Illingworth, G. D., Franx, M., & van Dokkum, P. G. 2006, *ApJ*, 653, 159
- Korn, A. J., Maraston, C., & Thomas, D. 2005, *A&A*, 438, 685
- Kuntschner, H. 2000, *MNRAS*, 315, 184
- Kuntschner, H., & Davies, R. L. 1998, *MNRAS*, 295, L29
- Kuntschner, H., Lucey, J. R., Smith, R. J., Hudson, M. J., & Davies, R. L. 2001, *MNRAS*, 323, 615
- Kuntschner, H., Smith, R. J., Colless, M., Davies, R. L., Kaldare, R., & Vazdekis, A. 2002, *MNRAS*, 337, 172
- Maraston, C. 1998, *MNRAS*, 300, 872

- Matković, A., & Guzmán, R. 2005, MNRAS, 362, 289
- Matteucci, F. 1994, A&A, 288, 57
- Mehlert, D., Thomas, D., Saglia, R. P., Bender, R., & Wegner, G. 2003, A&A, 407, 423
- Michielsen, D., Boselli, A., Conselice, C. J., Toloba, E., Whiley, I. M., Aragon-Salamanca, A., Balcells, M., Cardiel, N., Cenarro, A. J., Gorgas, J., Peletier, R. F., & Vazdekis, A. 2007, ArXiv e-prints, 712
- Nelan, J. E., Smith, R. J., Hudson, M. J., Wegner, G. A., Lucey, J. R., Moore, S. A. W., Quinney, S. J., & Suntzeff, N. B. 2005, ApJ, 632, 137
- Pedraz, S., Gorgas, J., Cardiel, N., & Guzmán, R. 1998, Ap&SS, 632, 137
- Poggianti, B. M., Bridges, T. J., Carter, D., Mobasher, B., Doi, M., Iye, M., Kashikawa, N., Komiyama, Y., Okamura, S., Sekiguchi, M., Shimasaku, K., Yagi, M., & Yasuda, N. 2001a, ApJ, 563, 118
- Poggianti, B. M., Bridges, T. J., Carter, D., Mobasher, B., Doi, M., Iye, M., Kashikawa, N., Komiyama, Y., Okamura, S., Sekiguchi, M., Shimasaku, K., Yagi, M., & Yasuda, N. 2001b, ApJ, 563, 118
- Proctor, R. N., Forbes, D. A., Hau, G. K. T., Beasley, M. A., De Silva, G. M., Contreras, R., & Terlevich, A. I. 2004, MNRAS, 349, 1381
- Proctor, R. N., & Sansom, A. E. 2002, MNRAS, 333, 517
- Rakos, K., & Schombert, J. 2004, AJ, 127, 1502
- Sánchez-Blázquez, P., Gorgas, J., Cardiel, N., & González, J. J. 2006a, A&A, 457, 787
- Sánchez-Blázquez, P., Gorgas, J., Cardiel, N., & González, J. J. 2006b, A&A, 457, 809
- Smith, R. J., Marzke, R. O., Hornschemeier, A. E., Bridges, T. J., Hudson, M. J., Miller, N. A., Lucey, J. R., Vázquez, G. A., Carter, D., 2008, MNRAS, 386, L96
- Terlevich, A. I., & Forbes, D. A. 2002, MNRAS, 330, 547
- Terlevich, A. I., Kuntschner, H., Bower, R. G., Caldwell, N., & Sharples, R. M. 1999, MNRAS, 310, 445
- Terlevich, R., Davies, R. L., Faber, S. M., & Burstein, D. 1981, MNRAS, 196, 381
- Thomas, D., Maraston, C., & Bender, R. 2002, Ap&SS, 281, 371
- Thomas, D., Maraston, C., & Bender, R. 2003, MNRAS, 343, 279
- Thomas, D., Maraston, C., Bender, R., & Mendes de Oliveira, C. 2005, ApJ, 621, 673
- Thomas, D., Maraston, C., & Korn, A. 2004, MNRAS, 351, L19
- Trager, S. C., Faber, S. M., Worthey, G., & González, J. J. 2000a, AJ, 120, 165
- Trager, S. C., Faber, S. M., Worthey, G., & González, J. J. 2000b, AJ, 119, 1645
- Trager, S. C., Worthey, G., Faber, S. M., Burstein, D., & Gonzalez, J. J. 1998, ApJS, 116, 1
- Tripicco, M. J., & Bell, R. A. 1995, AJ, 110, 3035
- Worthey, G. 1994, ApJS, 95, 107
- Worthey, G., & Collobert, M. 2003, ApJ, 586, 17
- Worthey, G., Faber, S. M., & Gonzalez, J. J. 1992, ApJ, 398, 69
- Worthey, G., Faber, S. M., Gonzalez, J. J., & Burstein, D. 1994, ApJS, 94, 687
- Worthey, G., & Ottaviani, D. L. 1997, ApJS, 111, 377

TABLE 1
INDEX MEASUREMENTS

GMP	Ca4227	δ_{4227}	G4300	δ_{4300}	H γ_A	$\delta_{H\gamma A}$	H γ_F	$\delta_{H\gamma F}$	Fe4383	δ_{4383}	Ca4455	δ_{4455}	Fe4531	δ_{4531}	C ₂ 4668	$\delta_{C_2 4668}$	H β	$\delta_{H\beta}$
2478	0.972	0.124	4.413	0.214	-3.346	0.246	-0.298	0.147	2.817	0.317	0.343	0.162	2.473	0.234	2.134	0.450	2.359	0.143
2489	1.211	0.077	5.460	0.131	-5.220	0.174	-1.052	0.098	4.814	0.190	1.189	0.097	3.271	0.142	6.442	0.399	2.005	0.091
2510	1.213	0.095	5.216	0.162	-5.554	0.199	-1.392	0.116	5.145	0.228	1.231	0.117	3.411	0.169	6.436	0.376	1.927	0.105
2516	1.128	0.086	4.811	0.150	-4.761	0.189	-1.088	0.107	4.727	0.221	1.285	0.113	3.369	0.164	6.490	0.419	1.570	0.120
2529	1.406	0.079	4.618	0.141	-3.547	0.195	-0.421	0.114	3.915	0.238	0.919	0.120	2.203	0.177	3.696	0.388	1.772	0.106
2535	1.208	0.095	5.517	0.160	-5.635	0.205	-1.489	0.118	4.961	0.230	1.207	0.116	3.535	0.167	6.422	0.417	1.908	0.107
2541	1.165	0.103	5.426	0.174	-5.939	0.223	-1.660	0.129	5.029	0.248	1.253	0.128	3.178	0.184	6.970	0.419	1.495	0.114
2585	0.484	0.087	3.690	0.147	-2.300	0.170	-0.056	0.100	2.023	0.237	0.439	0.120	1.480	0.175	5.630	0.422	2.642	0.105
2603	0.665	0.076	3.827	0.133	-0.776	0.186	1.385	0.108	2.770	0.247	0.977	0.124	2.993	0.182	4.918	0.406	2.740	0.114
2654	1.147	0.095	5.689	0.160	-5.897	0.195	-1.637	0.112	5.038	0.216	1.217	0.111	3.146	0.161	6.261	0.413	1.682	0.109
2692	1.091	0.081	4.449	0.145	-2.010	0.172	0.967	0.099	3.373	0.220	0.369	0.113	2.536	0.163	3.218	0.408	2.161	0.108
2778	1.163	0.074	4.968	0.130	-4.209	0.172	-0.126	0.091	4.916	0.180	1.155	0.094	3.831	0.134	6.025	0.383	1.933	0.091
2784	0.682	0.116	2.371	0.210	-3.481	0.227	-0.376	0.136	4.613	0.304	0.120	0.164	1.764	0.241	5.024	0.476	1.182	0.174
2799	1.679	0.099	4.730	0.177	-1.879	0.215	1.169	0.123	4.549	0.273	1.028	0.142	3.198	0.205	4.476	0.467	1.203	0.149
2805	1.453	0.091	5.237	0.157	-5.282	0.204	-1.169	0.115	4.954	0.214	1.277	0.108	3.518	0.157	7.224	0.409	1.729	0.099
2839	1.096	0.085	4.800	0.147	-4.592	0.184	-0.962	0.103	4.733	0.202	1.324	0.103	3.216	0.150	7.421	0.397	2.004	0.098
2852	1.418	0.102	4.861	0.183	-4.457	0.222	-0.781	0.130	4.525	0.255	1.809	0.126	3.103	0.188	5.181	0.437	2.129	0.139
2861	1.175	0.096	5.606	0.162	-5.780	0.207	-1.373	0.119	5.100	0.235	1.461	0.119	3.251	0.174	7.020	0.410	1.841	0.105
2879	1.460	0.090	4.963	0.161	-3.993	0.200	-1.425	0.121	1.784	0.257	0.504	0.125	1.977	0.185	2.856	0.443	1.714	0.121
2912	1.363	0.081	5.341	0.140	-5.654	0.179	-1.340	0.101	5.347	0.196	1.373	0.101	3.423	0.147	6.590	0.401	1.890	0.099
2922	1.269	0.113	5.368	0.193	-5.629	0.239	-1.462	0.139	5.392	0.270	1.435	0.138	3.162	0.201	7.772	0.437	1.649	0.121
2940	1.153	0.098	5.388	0.167	-5.245	0.212	-1.319	0.123	4.761	0.230	1.349	0.118	3.410	0.170	6.959	0.412	1.727	0.115
2960	1.227	0.067	4.709	0.120	-4.175	0.159	-0.491	0.086	4.352	0.176	0.856	0.090	3.268	0.130	4.420	0.399	2.105	0.083
2985	0.802	0.114	5.232	0.196	-3.378	0.247	0.224	0.142	3.443	0.340	0.187	0.177	3.174	0.253	4.962	0.508	1.544	0.169
3017	1.497	0.094	4.559	0.168	-3.308	0.206	-0.389	0.121	3.734	0.262	0.261	0.138	3.555	0.192	3.049	0.464	2.529	0.124
3058	1.014	0.068	3.291	0.124	-2.581	0.151	-0.003	0.086	3.661	0.186	1.243	0.094	2.194	0.144	2.683	0.415	2.042	0.092
3068	0.985	0.092	5.739	0.152	-6.077	0.199	-1.298	0.113	5.816	0.224	1.420	0.115	3.419	0.168	5.541	0.408	1.569	0.110
3073	1.162	0.097	5.593	0.164	-6.237	0.207	-1.737	0.120	5.244	0.225	1.186	0.117	3.343	0.169	7.065	0.382	1.756	0.112
3121	1.777	0.100	5.166	0.178	-4.600	0.221	-1.269	0.132	5.103	0.268	0.587	0.141	2.654	0.203	3.481	0.459	1.534	0.130
3126	0.989	0.092	4.409	0.162	-3.214	0.193	-0.111	0.113	5.406	0.236	1.201	0.122	2.692	0.181	3.920	0.417	1.784	0.118
3133	1.476	0.104	5.773	0.179	-6.601	0.230	-1.822	0.134	5.389	0.258	1.202	0.132	3.267	0.193	5.064	0.337	1.703	0.124
3166	1.571	0.116	5.255	0.216	-3.518	0.254	-0.394	0.152	1.646	0.352	-0.182	0.183	2.323	0.255	2.333	0.491	2.281	0.167
3170	1.120	0.098	5.315	0.165	-5.849	0.210	-1.567	0.123	5.382	0.241	1.561	0.123	3.249	0.183	6.614	0.339	1.934	0.124
3196	1.244	0.077	4.442	0.139	-4.208	0.177	-0.778	0.102	4.281	0.218	0.923	0.112	3.617	0.160	4.436	0.424	1.419	0.113
3201	1.192	0.087	5.302	0.151	-5.453	0.197	-1.444	0.114	4.878	0.234	1.208	0.120	3.031	0.175	6.472	0.427	2.050	0.111
3205	0.906	0.074	5.408	0.123	-3.872	0.171	-0.450	0.094	3.619	0.194	1.490	0.096	2.700	0.143	4.413	0.411	1.661	0.091
3206	1.464	0.069	5.296	0.123	-4.631	0.163	-0.891	0.092	4.022	0.187	1.311	0.095	3.400	0.136	4.886	0.401	1.815	0.093
3209	0.835	0.126	5.238	0.212	-1.904	0.259	1.296	0.149	2.374	0.360	-0.185	0.196	0.951	0.278	1.017	0.557	1.717	0.188
3213	1.084	0.099	5.134	0.167	-5.236	0.201	-1.340	0.115	5.205	0.217	1.262	0.112	3.384	0.160	6.073	0.416	1.497	0.121
3222	1.122	0.077	5.502	0.132	-5.706	0.171	-1.566	0.097	5.094	0.189	1.252	0.097	3.062	0.142	5.270	0.403	1.503	0.119
3254	1.370	0.114	4.195	0.202	-4.702	0.237	-1.337	0.143	4.734	0.283	0.966	0.146	3.269	0.209	5.555	0.452	1.418	0.133
3269	1.025	0.097	5.319	0.166	-5.353	0.210	-1.041	0.122	5.229	0.244	1.276	0.126	2.830	0.186	5.657	0.413	2.155	0.112
3292	0.343	0.069	4.828	0.117	-4.908	0.163	-1.446	0.090	3.791	0.189	2.019	0.090	3.639	0.137	3.534	0.392	1.357	0.097
3296	1.184	0.108	5.636	0.180	-5.663	0.226	-1.552	0.132	4.763	0.244	1.351	0.123	3.383	0.178	6.478	0.402	1.678	0.116
3312	0.638	0.092	4.247	0.155	-2.162	0.181	-0.181	0.108	2.474	0.248	0.658	0.123	2.562	0.180	2.610	0.440	1.083	0.113
3313	1.134	0.064	5.527	0.110	-4.536	0.156	-1.023	0.085	3.647	0.173	1.174	0.085	2.703	0.127	4.587	0.398	1.694	0.075
3336	1.441	0.107	4.524	0.184	-4.473	0.227	-1.215	0.135	4.022	0.286	1.603	0.144	2.832	0.214	5.661	0.468	1.979	0.142
3339	0.850	0.089	4.619	0.154	-4.800	0.192	-1.044	0.110	4.596	0.222	0.988	0.114	2.767	0.164	5.593	0.422	1.900	0.099
3352	1.170	0.107	5.437	0.182	-5.742	0.225	-1.408	0.130	5.414	0.252	1.454	0.130	3.567	0.191	7.383	0.430	1.745	0.125
3367	1.012	0.077	4.854	0.133	-5.014	0.174	-1.060	0.097	5.127	0.195	1.295	0.101	3.318	0.146	6.871	0.399	1.991	0.100
3400	1.184	0.095	5.020	0.164	-5.027	0.214	-1.209	0.120	4.980	0.234	1.138	0.122	3.240	0.175	6.901	0.398	1.808	0.109
3438	1.662	0.101	5.285	0.180	-2.202	0.221	0.863	0.127	3.396	0.296	-0.156	0.156	2.992	0.220	3.176	0.487	1.772	0.137
3471	1.006	0.073	5.329	0.123	-4.604	0.167	-0.944	0.093	4.629	0.184	1.456	0.092	3.054	0.137	5.553	0.399	1.425	0.087
3486	0.916	0.099	5.492	0.166	-4.708	0.212	-0.728	0.123	3.543	0.252	0.921	0.126	2.945	0.183	4.016	0.433	1.985	0.110
3510	1.256	0.109	5.608	0.183	-5.964	0.236	-1.762	0.137	5.254	0.264	1.425	0.135	3.418	0.194	7.630	0.437	1.310	0.127
3534	0.830	0.065	4.721	0.113	-3.604	0.147	-0.451	0.081	3.646	0.169	1.150	0.084	2.912	0.124	3.035	0.403	1.850	0.072
3554	0.829	0.070	4.704	0.121	-4.271	0.153	-0.742	0.086	4.117	0.178	0.922	0.090	2.616	0.132	4.782	0.392	1.797	0.082
3561	1.214	0.096	5.079	0.166	-5.097	0.216	-0.998	0.120	5.285	0.228	1.493	0.117	2.859	0.172	6.876	0.386	1.806	0.103
3565	0.684	0.119	3.926	0.209	-2.992	0.239	0.313	0.140	3.268	0.308	1.311	0.155	2.597	0.232	4.139	0.494	1.231	0.168
3645	1.770	0.105	4.871	0.193	-3.954	0.235	-0.772	0.136	3.264	0.280	0.769	0.143	3.340	0.204	6.710	0.454	0.856	0.121
3656	1.019	0.072	5.413	0.123	-4.768	0.159	-1.155	0.090	3.501	0.173	0.824	0.087	2.510	0.126	3.991	0.372	1.523	0.087
3681	1.149	0.082	5.780	0.141	-4.236	0.178	-0.919	0.102	2.368	0.218	0.472	0.110	3.615	0.153	4.010	0.420	2.496	0.1

TABLE 1—*Continued*

GMP	Ca4227	δ_{4227}	G4300	δ_{4300}	H γ_A	$\delta_{H\gamma A}$	H γ_F	$\delta_{H\gamma F}$	Fe4383	δ_{4383}	Ca4455	δ_{4455}	Fe4531	δ_{4531}	C24668	δ_{C24668}	H β	$\delta_{H\beta}$
3739	1.159	0.099	5.695	0.166	-6.208	0.216	-1.884	0.124	5.128	0.260	1.377	0.133	3.397	0.193	6.874	0.442	1.557	0.111
3761	1.349	0.095	5.465	0.162	-5.464	0.195	-1.213	0.111	5.189	0.218	1.405	0.111	3.322	0.161	6.686	0.395	1.878	0.117
3780	1.049	0.102	5.442	0.175	-4.562	0.214	-0.601	0.124	3.853	0.259	0.618	0.135	3.214	0.192	4.018	0.429	2.130	0.126
3782	1.212	0.072	5.410	0.124	-5.514	0.172	-1.301	0.095	4.728	0.172	1.215	0.088	3.392	0.126	6.014	0.392	1.733	0.079
3792	1.330	0.103	5.472	0.175	-6.265	0.221	-1.918	0.129
3794	1.084	0.094	5.417	0.159	-5.270	0.203	-1.534	0.117	4.244	0.236	1.114	0.120	3.309	0.171	5.585	0.426	1.528	0.116
3851	1.156	0.102	4.508	0.180	-4.298	0.212	-0.798	0.125	4.531	0.251	1.304	0.126	3.314	0.184	6.500	0.393	2.100	0.120
3855	1.345	0.092	3.140	0.172	-1.341	0.190	0.214	0.112	3.182	0.239	1.103	0.120	2.471	0.178	4.919	0.430	2.330	0.117
3914	1.027	0.096	5.167	0.163	-5.669	0.209	-1.731	0.120	4.475	0.230	1.291	0.117	3.184	0.169	6.836	0.415	1.676	0.107

TABLE 2
INDEX AND MODEL MEASUREMENTS

GMP	Fe5015	δ_{5015}	Mg ₁	δ_{Mg1}	Mg ₂	δ_{Mg2}	Mg _b	δ_{Mgb}	Fe5270	δ_{5270}	Fe5335	δ_{5335}	Age	δ_{Age}	[Z/H]	$\delta_{[Z/H]}$	[α /Fe]	$\delta_{[\alpha/Fe]}$	SNR	
2478	3.629	0.364	0.027	0.013	0.146	0.012	2.966	0.163	2.031	0.199	2.463	0.237	3.8	1.5	-0.108	0.093	0.145	0.075	28	
2489	4.799	0.210	0.075	0.012	0.213	0.015	3.963	0.095	2.555	0.112	2.398	0.135	5.5	1.6	0.133	0.076	0.26	0.032	54	
2510	5.257	0.279	0.088	0.012	0.227	0.011	4.074	0.116	2.797	0.141	2.594	0.170	5.5	1.3	0.183	0.078	0.198	0.047	48	
2516	5.229	0.273	0.112	0.012	0.254	0.016	4.141	0.131	2.723	0.152	2.565	0.181	46	
2529	3.202	0.296	0.031	0.012	0.131	0.011	2.913	0.123	2.262	0.152	2.133	0.183	10.7	0.8	-0.313	0.067	0.163	0.038	28	
2535	4.328	0.265	0.091	0.012	0.240	0.014	4.368	0.116	2.686	0.136	2.440	0.163	5.6	2.2	0.214	0.126	0.303	0.038	47	
2541	4.954	0.287	0.115	0.012	0.263	0.014	4.692	0.124	2.621	0.147	2.344	0.178	13.5	0.7	0.063	0.052	0.35	0.027	45	
2585	5.684	0.266	0.020	0.012	0.116	0.015	2.294	0.127	1.080	0.153	1.509	0.183	5.9	1	-0.714	0.102	0.478	0.079	23	
2603	4.875	0.299	0.020	0.012	0.115	0.012	2.355	0.133	2.248	0.159	2.353	0.192	2	0.7	39	
2654	4.671	0.255	0.101	0.012	0.236	0.015	4.042	0.113	2.710	0.131	2.437	0.158	10.1	2.5	0.037	0.077	0.2	0.042	51	
2692	3.401	0.289	0.022	0.012	0.138	0.013	2.970	0.121	2.076	0.146	2.257	0.175	6	1.3	-0.195	0.055	0.184	0.06	26	
2778	5.554	0.208	0.062	0.011	0.171	0.016	3.612	0.101	2.478	0.116	2.583	0.138	8	3.6	-0.021	0.112	0.135	0.041	34	
2784	5.775	0.386	0.040	0.013	0.156	0.014	2.481	0.190	0.974	0.232	2.565	0.262	15	
2799	4.358	0.335	0.022	0.012	0.142	0.016	3.265	0.161	1.490	0.192	1.063	0.233	17	
2805	4.983	0.233	0.083	0.011	0.224	0.016	3.693	0.111	2.661	0.127	2.681	0.151	11.6	2	-0.039	0.066	0.089	0.047	48	
2839	4.929	0.214	0.112	0.011	0.254	0.016	4.310	0.104	2.684	0.118	2.583	0.140	4.4	1.8	0.265	0.144	0.275	0.04	53	
2852	4.426	0.334	0.049	0.012	0.176	0.015	3.373	0.151	3.220	0.175	2.158	0.214	3.8	1.7	0.175	0.131	0.083	0.06	27	
2861	4.801	0.268	0.086	0.012	0.217	0.014	3.661	0.117	3.136	0.135	2.550	0.164	5.7	2.7	0.171	0.123	0.067	0.041	53	
2879	4.378	0.300	0.047	0.012	0.159	0.015	2.638	0.137	1.493	0.162	2.695	0.189	23	
2912	5.394	0.229	0.092	0.012	0.241	0.015	4.289	0.103	2.989	0.120	2.787	0.144	4	1.5	0.378	0.109	0.198	0.039	54	
2922	5.080	0.300	0.121	0.012	0.270	0.015	4.615	0.134	2.833	0.156	2.752	0.187	10.4	3.1	0.209	0.116	0.242	0.043	45	
2940	4.549	0.279	0.101	0.012	0.250	0.014	4.240	0.123	2.548	0.145	2.485	0.174	11	2.9	0.038	0.091	0.261	0.043	45	
2960	4.880	0.197	0.048	0.011	0.164	0.016	2.987	0.098	2.686	0.110	2.114	0.134	5.3	1.4	-0.107	0.051	0.075	0.04	45	
2985	2.363	0.408	0.034	0.012	0.118	0.017	1.529	0.206	1.624	0.232	2.531	0.268	15	
3017	5.024	0.313	0.038	0.012	0.137	0.016	2.016	0.154	2.763	0.174	1.377	0.218	3	0.7	-0.272	0.078	22	
3058	3.766	0.219	0.050	0.011	0.165	0.016	2.574	0.109	2.856	0.121	2.882	0.145	5.3	1.6	23	
3068	4.431	0.282	0.073	0.012	0.204	0.013	3.757	0.120	2.811	0.142	2.404	0.173	12.9	0.5	-0.084	0.049	0.132	0.048	44	
3073	5.151	0.286	0.112	0.012	0.266	0.012	4.389	0.121	2.854	0.144	3.015	0.172	9	2.7	0.281	0.081	0.17	0.04	45	
3121	4.478	0.368	0.038	0.013	0.169	0.015	2.844	0.174	2.057	0.203	1.544	0.249	24	
3126	3.529	0.314	0.046	0.012	0.160	0.014	3.518	0.134	3.017	0.159	2.148	0.196	10	2.8	-0.051	0.097	0.093	0.063	26	
3133	4.732	0.294	0.062	0.011	0.204	0.010	4.174	0.133	3.106	0.167	2.553	0.195	7.7	3.1	0.224	0.117	0.166	0.053	35	
3166	1.735	0.422	0.021	0.013	0.095	0.013	2.382	0.193	2.517	0.227	2.745	0.274	3.7	1.6	-0.163	0.092	16	
3170	5.347	0.306	0.099	0.011	0.243	0.010	4.136	0.139	2.673	0.173	2.697	0.201	5.4	2.2	0.195	0.134	0.214	0.046	41	
3196	4.151	0.269	0.063	0.012	0.166	0.015	3.080	0.125	2.229	0.145	1.424	0.185	19	
3201	4.621	0.266	0.101	0.012	0.226	0.015	3.639	0.125	2.668	0.144	2.813	0.171	3.7	1.5	0.188	0.088	0.109	0.044	45	
3205	4.661	0.216	0.035	0.012	0.141	0.015	2.194	0.107	1.958	0.120	2.617	0.142	25	
3206	4.141	0.222	0.076	0.012	0.197	0.015	3.526	0.098	2.010	0.116	1.670	0.142	11.9	1.8	-0.283	0.039	0.481	0.055	33	
3209	0.648	0.472	0.004	0.013	0.084	0.015	2.050	0.215	1.989	0.254	2.227	0.307	15	
3213	4.988	0.280	0.113	0.012	0.261	0.016	4.405	0.129	2.509	0.150	2.387	0.179	14.4	0.6	-0.028	0.025	0.313	0.04	48	
3222	4.024	0.289	0.110	0.012	0.250	0.016	4.441	0.129	2.491	0.153	1.884	0.186	14.7	0.6	-0.077	0.024	0.436	0.056	41	
3254	5.094	0.320	0.059	0.012	0.228	0.014	4.224	0.143	3.298	0.167	2.330	0.205	14.9	3.9	0.05	0.112	0.141	0.031	28	
3269	3.872	0.313	0.068	0.012	0.200	0.013	3.613	0.134	2.694	0.161	2.323	0.194	3	1.9	0.179	0.104	0.198	0.046	38	
3292	3.019	0.249	0.054	0.010	0.143	0.016	1.676	0.123	2.259	0.133	2.157	0.157	22	
3296	4.657	0.288	0.106	0.012	0.257	0.012	4.697	0.119	2.989	0.142	2.728	0.170	6.9	5	0.359	0.144	0.261	0.043	49	
3312	3.981	0.284	0.019	0.012	0.124	0.014	2.297	0.131	1.714	0.154	2.509	0.183	25	
3313	3.584	0.184	0.056	0.012	0.171	0.015	3.081	0.087	2.428	0.099	2.102	0.121	11.8	2.6	-0.282	0.041	0.166	0.05	49	
3336	5.272	0.351	0.111	0.013	0.254	0.016	2.998	0.175	2.568	0.192	1.916	0.234	8	2.6	-0.196	0.088	0.148	0.078	19	
3339	3.370	0.238	0.054	0.012	0.180	0.015	3.511	0.110	2.842	0.127	2.298	0.154	5.7	4	0.051	0.131	0.123	0.047	33	
3352	42
3367	5.059	0.243	0.139	0.011	0.273	0.016	4.309	0.118	2.301	0.137	2.458	0.161	5.6	2.4	0.146	0.127	0.358	0.026	45	
3400	51
3438	3.396	0.331	0.023	0.012	0.133	0.016	2.475	0.163	1.006	0.195	1.329	0.229	15	
3471	4.151	0.210	0.067	0.012	0.193	0.015	3.575	0.094	2.580	0.109	2.075	0.133	-0.209	0.019	0.24	0.043	49	
3486	2.676	0.301	0.040	0.012	0.150	0.013	3.560	0.126	2.781	0.151	2.750	0.183	4.4	1.8	0.123	0.089	0.068	0.044	32	
3510	4.528	0.289	0.135	0.012	0.292	0.016	4.943	0.129	2.959	0.149	2.675	0.178	0.219	0.035	0.285	0.037	46	
3534	4.351	0.180	0.051	0.011	0.165	0.016	2.916	0.088	2.452	0.100	2.551	0.120	10.1	2.5	-0.241	0.041	0.005	0.032	43	
3554	3.508	0.231	0.050	0.012	0.165	0.014	3.165	0.098	2.399	0.116	2.105	0.142	11	2	-0.248	0.043	0.186	0.054	43	
3561	58
3565	6.408	0.374	0.066	0.013	0.178	0.015	3.373	0.183	2.086	0.219	2.164	0.262	15	
3645	4.129	0.299	0.086	0.012	0.231	0.016	3.258	0.146	2.273	0.167	2.183	0.199	25	
3656	4.059	0.246	0.061	0.012	0.199	0.013	3.604	0.100	2.557	0.120	2.030	0.148	-0.211	0.021	0.262	0.048	53	
3681	5.865	0.280	0.045	0.012	0.152	0.016	2.884	0.134	2.805	0.156	2.266	0.189	2.4	0.5	0.126	0.032	0.038	0.043	21	
3706	4.526	0.266	0.071	0.012	0.204	0.015	3.752	0.120	2.474	0.141	2.449	0.170	4.6	3.3	0.076	0.113	0.219	0.046	49	
3707	4.987	0.265	0.079	0.012	0.199	0.014	3.392	0.119	2.542	0.139	2.303	0.167	5.5	2.3	-0.053	0.119	0.15	0.045	38	
3733	5.147	0.279	0.138	0.012	0.299	0.016	4.894	0.129	2.672	0.151	2.542	0.178</						

TABLE 2—*Continued*

GMP	Fe5015	δ_{5015}	Mg ₁	δ_{Mg1}	Mg ₂	δ_{Mg2}	Mg _b	δ_{Mgb}	Fe5270	δ_{5270}	Fe5335	δ_{5335}	Age	δ_{Age}	[Z/H]	$\delta_{[Z/H]}$	[α /Fe]	$\delta_{[\alpha/Fe]}$	SNR	
3739	5.142	0.273	0.117	0.012	0.270	0.016	4.504	0.130	2.785	0.150	2.573	0.179	11.3	3.5	0.123	0.098	0.254	0.039	46	
3761	5.200	0.269	0.095	0.012	0.244	0.013	4.249	0.114	2.855	0.135	2.707	0.163	5.8	1.5	0.252	0.115	0.206	0.039	49	
3780	3.488	0.306	0.045	0.012	0.155	0.013	3.505	0.130	2.240	0.159	1.977	0.193	5.3	2.4	-0.073	0.139	0.32	0.062	30	
3782	4.925	0.209	0.093	0.012	0.237	0.015	4.085	0.098	2.703	0.114	2.319	0.138	8.7	3.4	0.055	0.099	0.241	0.032	56	
3792	41
3794	4.574	0.268	0.109	0.012	0.253	0.014	4.529	0.119	2.643	0.140	2.373	0.169	12.9	0.8	0.051	0.057	0.313	0.039	47	
3851	4.167	0.306	0.063	0.012	0.187	0.013	3.626	0.130	3.031	0.156	2.484	0.189	3	1.1	0.26	0.107	0.118	0.047	41	
3855	3.443	0.266	0.055	0.011	0.151	0.016	3.693	0.128	1.424	0.153	2.715	0.177	3	2.1	0.179	0.28	0.397	0.047	22	
3914	4.973	0.251	0.112	0.011	0.257	0.016	4.386	0.120	2.793	0.137	2.728	0.163	10.4	2.5	0.145	0.112	0.207	0.043	46	

TABLE 3
COMPARISON WITH OTHER STUDIES

Index	Ref.	$\langle \Delta I \rangle$	std	σ_{exp}
Ca4227	P01	-0.111 ± 0.129	0.755	0.341
	N05	-0.207 ± 0.047	0.236	0.228
	S08	0.098 ± 0.095	0.426	0.150
G4300	P01	-0.217 ± 0.264	1.519	0.567
	N05	0.020 ± 0.094	0.471	0.368
	S08	-0.146 ± 0.234	1.046	0.328
H γ_A	P01	0.212 ± 0.304	1.745	0.626
	N05	0.105 ± 0.114	0.569	0.508
	S08	0.359 ± 0.225	1.004	0.368
H γ_F	P01	-0.040 ± 0.162	0.945	0.397
	N05	0.037 ± 0.064	0.320	0.242
	S08	0.146 ± 0.146	0.653	0.207
Fe4383	P01	-0.970 ± 0.275	1.604	0.789
	N05	0.154 ± 0.139	0.697	0.466
	S08	-0.113 ± 0.205	0.916	0.420
Ca4455	P01	-0.259 ± 0.116	0.677	0.395
	N05	-0.001 ± 0.038	0.189	0.194
	S08	-0.089 ± 0.122	0.547	0.194
Fe4531	P01	-0.193 ± 0.153	0.890	0.573
	N05	-0.152 ± 0.066	0.328	0.303
	S08	-0.206 ± 0.149	0.668	0.318
C $_2$ 4668	P01	-0.236 ± 0.345	2.010	0.928
	N05	0.154 ± 0.139	0.697	0.626
	S08	0.140 ± 0.232	1.037	0.650
H β	P01	0.129 ± 0.125	0.729	0.349
	N05	0.071 ± 0.042	0.210	0.163
	S08	-0.118 ± 0.095	0.424	0.205
Fe5015	P01	-0.652 ± 0.208	1.215	0.717
	N05	-0.313 ± 0.102	0.477	0.421
	S08	-0.243 ± 0.246	1.098	0.805
Mg $_1$	P01	-0.012 ± 0.006	0.037	0.014
	N05	-0.023 ± 0.002	0.010	0.014
	S08	-0.014 ± 0.003	0.014	0.013
Mg $_2$	P01	0.004 ± 0.007	0.041	0.017
	N05	-0.017 ± 0.002	0.010	0.017
	S08	-0.018 ± 0.004	0.018	0.015
Mg $_b$	P01	0.015 ± 0.119	0.692	0.339
	N05	-0.051 ± 0.041	0.193	0.173
	S08	-0.015 ± 0.115	0.513	0.213
Fe5270	P01	-0.178 ± 0.112	0.652	0.380
	N05	-0.018 ± 0.051	0.241	0.196
	S08	-0.334 ± 0.127	0.567	0.240
Fe5335	P01	0.074 ± 0.098	0.572	0.430
	N05	-0.065 ± 0.050	0.233	0.226
	S08	0.058 ± 0.146	0.653	0.276

NOTE.—Comparison of line strengths measured in this and other studies. Ref.: reference in the literature where P01 is from Poggianti et al. (2001a), N05 is from Nelan et al. (2005) and S08 is from Smith et al. (2008); $\langle \Delta I \rangle$: mean offset between our study and other ($I_{here} - I_{other}$) and the error in the mean; *std* standard deviation of the differences; σ_{exp} : standard deviation expected from the errors.

TABLE 4
 $I - \sigma$ LINEAR FITS

Index	Intercept $_{<100}$	Slope $_{<100}$	$\rho_{<100}$	Intercept $_{\geq 100}$	Slope $_{\geq 100}$	$\rho_{\geq 100}$
Ca4227	0.828 ± 0.640	0.139 ± 0.352	0.063	0.029 ± 0.590	0.494 ± 0.268	0.187
G4300	-0.586 ± 1.717	2.974 ± 0.944	0.544	4.746 ± 1.140	0.285 ± 0.519	-0.028
H γ_A	7.165 ± 3.017	-6.110 ± 1.658	-0.652	-3.034 ± 1.852	-1.194 ± 0.843	-0.170
H γ_F	4.644 ± 1.620	-2.836 ± 0.890	-0.612	0.369 ± 0.834	-0.834 ± 0.380	-0.290
Fe4383	-3.367 ± 1.731	4.093 ± 0.951	0.594	4.511 ± 1.091	0.234 ± 0.497	0.043
Ca4455	-0.854 ± 0.873	1.015 ± 0.480	0.371	1.773 ± 0.445	-0.235 ± 0.203	-0.087
Fe4531	-0.629 ± 1.040	1.962 ± 0.572	0.426	2.773 ± 0.606	0.216 ± 0.276	0.016
C ₂ 4668	-3.648 ± 2.460	4.623 ± 1.352	0.491	-3.203 ± 2.079	4.450 ± 0.947	0.547
H β	3.885 ± 0.945	-1.070 ± 0.519	-0.363	2.939 ± 0.510	-0.596 ± 0.233	-0.254
Fe5015	2.792 ± 1.920	0.782 ± 1.055	0.163	4.102 ± 1.027	0.340 ± 0.469	0.032
Mg ₁	-0.135 ± 0.040	0.106 ± 0.022	0.684	-0.204 ± 0.036	0.141 ± 0.017	0.702
Mg ₂	-0.136 ± 0.063	0.171 ± 0.035	0.652	-0.143 ± 0.045	0.178 ± 0.020	0.717
Mgb	-0.943 ± 0.981	2.292 ± 0.539	0.532	-0.436 ± 0.743	2.120 ± 0.340	0.667
Fe5270	0.151 ± 0.945	1.303 ± 0.519	0.257	3.236 ± 0.650	-0.243 ± 0.297	-0.062
Fe5335	0.985 ± 0.952	0.730 ± 0.523	0.103	2.472 ± 0.640	0.021 ± 0.292	0.156
(Fe)	0.568 ± 0.813	1.017 ± 0.447	0.254	2.854 ± 0.586	-0.111 ± 0.268	-0.003
[MgFe]'	-0.255 ± 0.708	1.683 ± 0.389	0.513	1.743 ± 0.536	0.726 ± 0.245	0.387

NOTE.— $I - \sigma$ Linear Fits for low- and high- σ early-type galaxies. The intercept and slope of the $I - \sigma$ linear fit, and Spearman Rank correlation coefficient (ρ), are presented for low- and for high- σ galaxies respectively. Note that the correlation coefficients are low for galaxies in group I implying that for these indices the $I - \sigma$ relations are not significant.

TABLE 5
 $I - \sigma$ STATISTICS FOR GROUP IA

Index	N $_{<100}$	N $_{\geq 100}$	$\bar{I}_{<100}$	$\bar{I}_{\geq 100}$	std $_{<100}$	std $_{\geq 100}$	prob $_{KS}$
G4300	41	70	4.813	5.372	0.861	0.482	3.75E-06
Fe4383	41	69	4.063	5.024	0.950	0.453	1.15E-09
Ca4455	41	69	0.988	1.258	0.413	0.186	5.82E-04
Fe4531	41	69	2.932	3.246	0.532	0.251	2.48E-04
Fe5270	41	66	2.516	2.704	0.456	0.260	8.01E-04

NOTE.—Statistics for group Ia of $I - \sigma$ plots. N: number of galaxies with $\sigma < 100$ km s $^{-1}$ and with $\sigma \geq 100$ km s $^{-1}$ excluding the “off-grid galaxies”; \bar{I} : average value of the index for low- and high- σ galaxies; std $_{<100}$ and std $_{\geq 100}$: standard deviation of the points for the low- and high- σ galaxies; prob $_{KS}$: the KS probability that the two sets are drawn from the same distribution.

TABLE 6
 $I - \sigma$ LINEAR FITS AND STATISTICS FOR INDEX GROUP IB

Index	N	Intercept	Slope	ρ	$\sigma_{Int}<100$	$\sigma_{Err}<100$	$\sigma_{Int}\geq 100$	$\sigma_{Err}\geq 100$	prob $_{KS}$
C4227	111	0.614 ± 0.099	0.262 ± 0.049	0.159	0.197	0.217	0.242	0.256	0.200
Fe5015	107	1.940 ± 0.282	1.313 ± 0.136	0.355	0.624	0.291	0.000	0.428	0.000
Fe5335	107	1.523 ± 0.158	0.449 ± 0.074	0.331	0.297	0.162	0.199	0.169	0.531
(Fe)	107	1.508 ± 0.104	0.506 ± 0.048	0.329	0.283	0.099	0.374	0.147	0.913

NOTE.—Statistics for group Ib of $I - \sigma$ plots. N: number of galaxies; Intercept and Slope: linear regression applied to all the galaxies; ρ : Spearman-Rank correlation coefficient; σ_{Int} : intrinsic scatter for the two sub-samples, i.e. standard deviation of residuals between the points and the linear fit for each sub-sample of galaxies (low and high- σ); σ_{Err} : scatter due to the errors; prob $_{KS}$: the KS probability that the two sets are drawn from the same distribution.

TABLE 7

 $I - \sigma$ LINEAR FITS AND STATISTICS FOR INDEX GROUP II AND BALMER LINES

Index	N	Intercept	Slope	σ_{Int}	σ_{Err}	ρ
C ₂ 4668	110	-3.890 ± 0.415	4.782 ± 0.197	0.750	0.972	0.524
Mg ₁	107	-0.177 ± 0.010	0.128 ± 0.004	0.844	0.016	0.011
Mg ₂	107	-0.186 ± 0.012	0.197 ± 0.006	0.871	0.023	0.014
Mgb	107	-1.157 ± 0.134	2.435 ± 0.062	0.854	0.359	0.167
[MgFe]'	107	0.508 ± 0.081	1.290 ± 0.040	0.729	0.372	0.112
H γ_A	111	3.503 ± 0.229	-4.160 ± 0.109	-0.665	1.357	0.565
H γ_F	111	3.563 ± 0.126	-2.286 ± 0.059	-0.709	0.684	0.297
H β	110	3.706 ± 0.100	-0.943 ± 0.047	-0.502	0.380	0.190

NOTE.—Statistics for group II of $I - \sigma$ plots and Balmer lines. N: number of galaxies; Intercept and slope of the linear fit which takes into account both the uncertainties in the index and velocity dispersion; ρ : Spearman-Rank correlation coefficient; σ_{Int} : intrinsic scatter; σ_{Err} : scatter due to the errors.

TABLE 8

VELOCITY DISPERSIONS, AGES, METALLICITIES AND $[\alpha/Fe]$ FOR BINNED GALAXIES

Bin	N	$\log \sigma$ Range	$\langle \log \sigma \rangle$	$\langle \log \text{Age} \rangle$	$\langle [Z/H] \rangle$	$\langle [\alpha/Fe] \rangle$
1	5	$2.291 \leq \sigma < 2.127$	0.893 ± 0.092	0.150 ± 0.069	0.255 ± 0.035	2.212 ± 0.020
2	12	$2.127 \leq \sigma < 1.963$	0.880 ± 0.064	0.086 ± 0.027	0.202 ± 0.023	2.053 ± 0.016
3	8	$1.963 \leq \sigma < 1.799$	0.765 ± 0.102	-0.041 ± 0.078	0.179 ± 0.048	1.890 ± 0.016
4	13	$1.799 \leq \sigma < 1.635$	0.721 ± 0.066	-0.085 ± 0.043	0.162 ± 0.037	1.744 ± 0.008
5	4	$1.635 \leq \sigma < 1.400$	0.778 ± 0.094	-0.111 ± 0.147	0.143 ± 0.031	1.610 ± 0.010

TABLE 9

MODEL PARAMETERS VS. σ RELATIONS

	Intercept	Slope
$\log \text{Age vs. } \sigma$	0.22 ± 0.34	0.31 ± 0.18
$[Z/H] \text{ vs. } \sigma$	-1.00 ± 0.26	0.53 ± 0.13
$[\alpha/H] \text{ vs. } \sigma$	-0.13 ± 0.13	0.17 ± 0.07

TABLE 10

RELATIONS BETWEEN AGE AND METALLICITY

$[Z/H] = a + b \cdot \log \text{Age}$	Intercept	Slope	ρ
High- σ	0.795 ± 0.143	-0.723 ± 0.128	-0.750
Low- σ	0.482 ± 0.105	-0.744 ± 0.119	-0.594

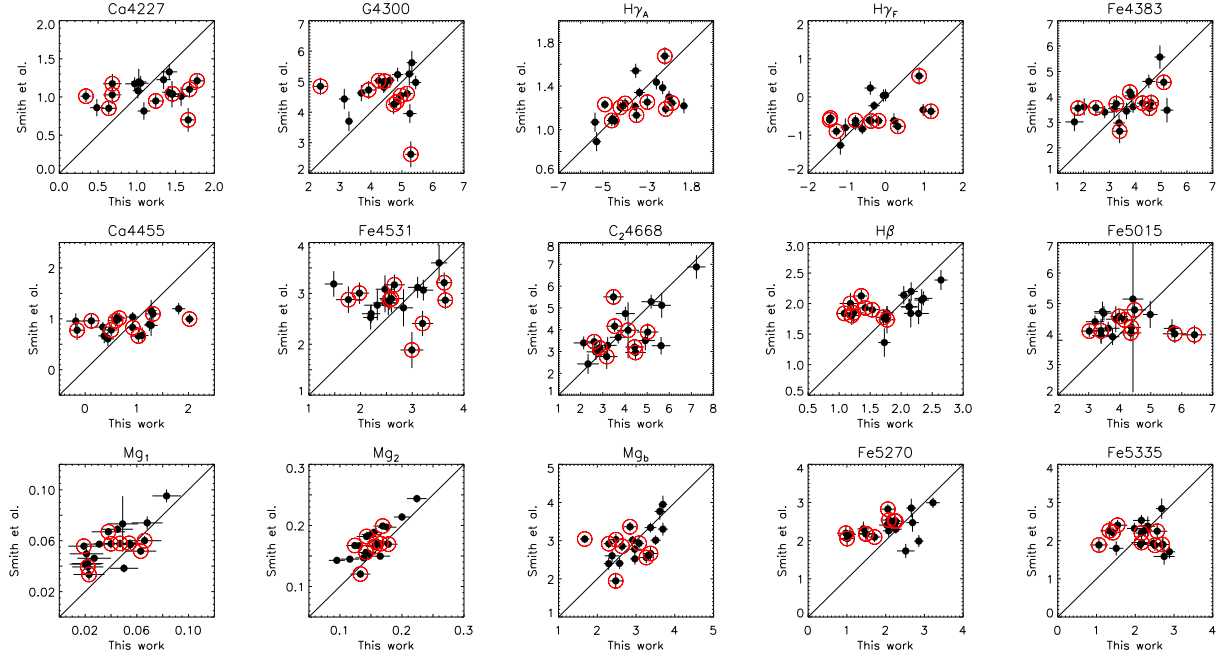


Fig. 1.— Comparison of our sample with Smith et al. (2008). The lines have a slope of 1.0 and indicate a one-to-one agreement between the two data sets. Galaxies which do not fit on the model grids, the “off-grid” galaxies, are labeled as red open circles and are discussed in § 6.1.

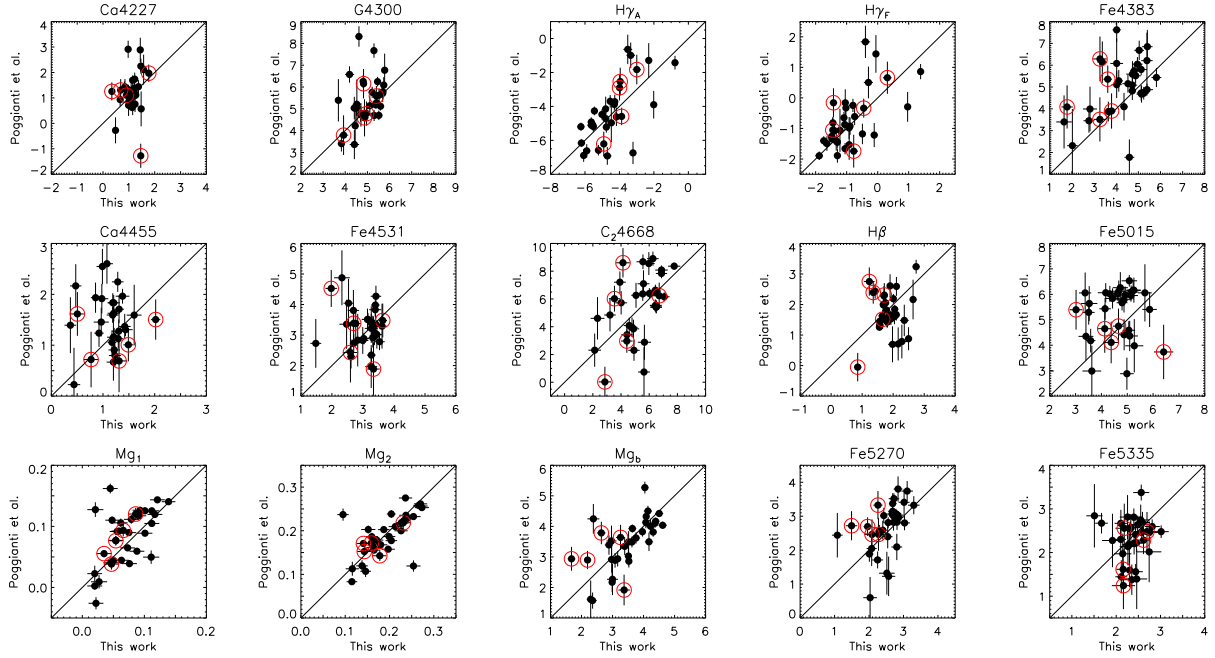


Fig. 2.— Comparison of our sample with Poggianti et al. (2001a) represented as solid circles. Symbols and lines are the same as in Figure 1.

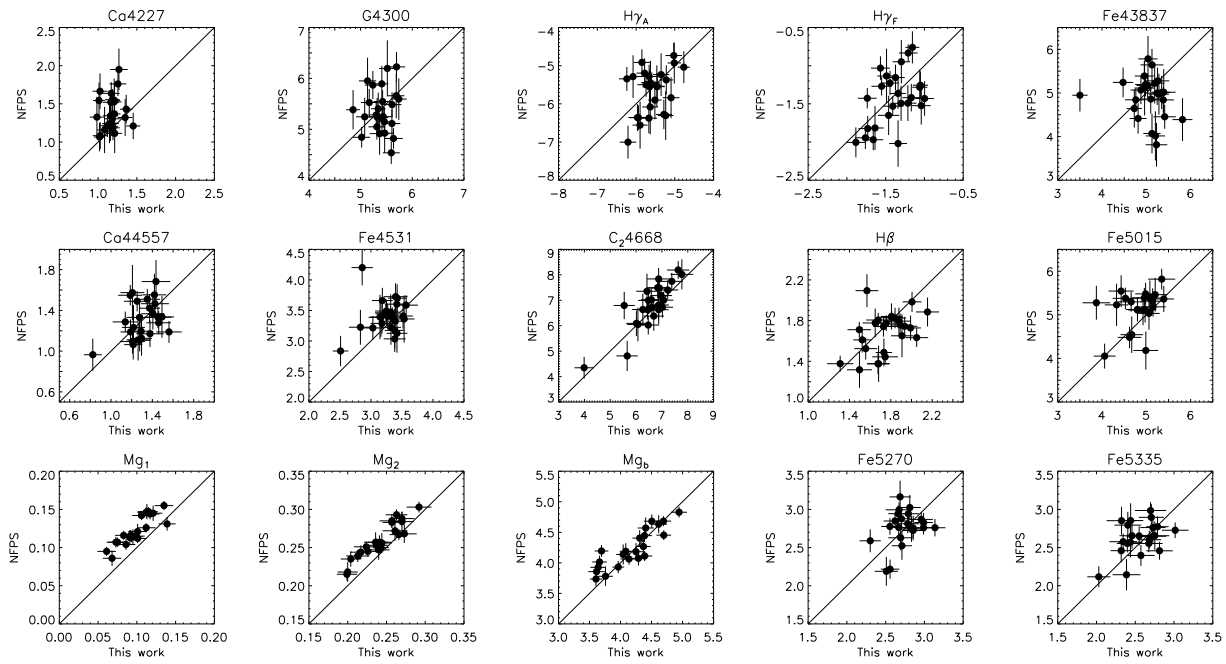


Fig. 3.— Comparison of our sample with Nelan et al. (2005). Symbols and lines are the same as in Figure 1.

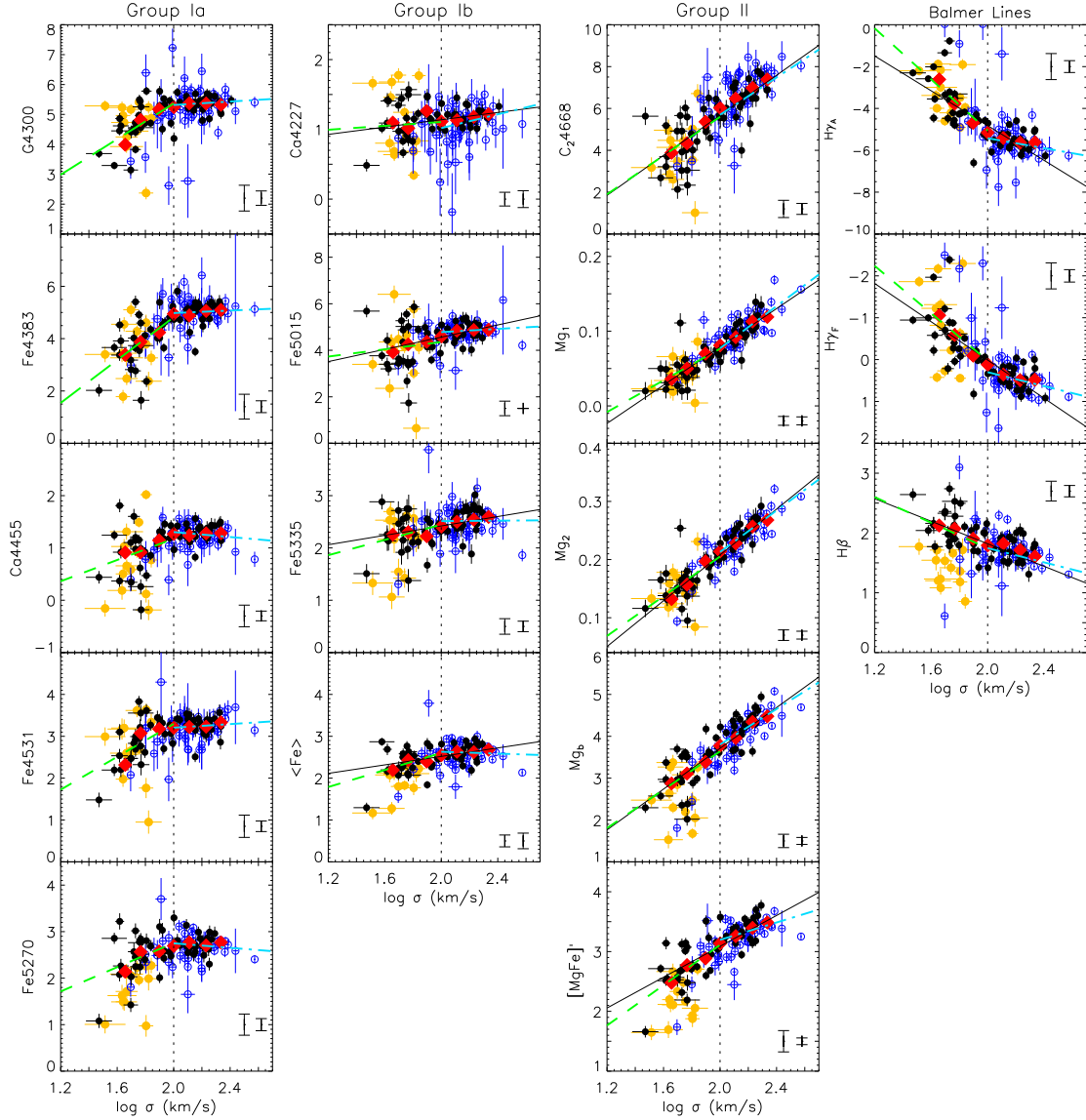


Fig. 4.— Index – $\log \sigma$ plots. Data from the NFPS sample are marked by blue open circles, and our sample with black filled circles and yellow circles for galaxies not fitted by models. We binned the data by σ where each bin contains an equal number of objects. The red diamonds are weighted average values of each bin. The vertical dotted line corresponds to $\sigma = 100 \text{ km s}^{-1}$. Group Ia and Ib represent the set of $I - \sigma$ relations that show evidence for a break in the slope, group II $I - \sigma$ with strong linear relations, and the last column contains Balmer lines. In the bottom right corner of $I - \sigma$ plots in Group Ia we show the 1-sigma scatter for low- σ on the left and high- σ galaxies on the right. In the case of Group Ib and Balmer lines these lines correspond to the intrinsic scatter for low- and high- σ respectively. For Group II, we show the intrinsic and observed scatter, respectively, in the bottom right corner. The black lines represent linear fits for all the galaxies in the individual $I - \sigma$ figures, while the green dashed and light blue dash-dotted lines mark linear fits to low- and high- σ galaxies respectively. Note that the “off-grid” galaxies were not included in the bins and linear regression calculations.

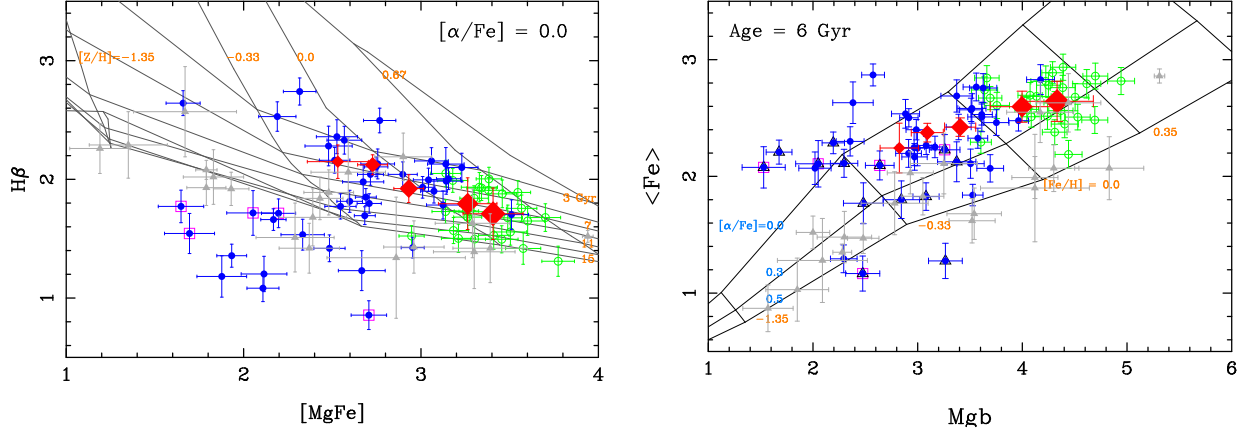


Fig. 5.— $[MgFe]'$ vs. $H\beta$ and Mgb vs. $\langle Fe \rangle$ plots for age of 6 Gyr plot. The low- and high- σ galaxies are represented by the blue solid and green open circles, respectively. We mark the nucleated dEs (Graham & Guzmán 2003) with purple open squares. The large red solid diamonds denote the galaxies binned by velocity dispersion where each bin is of an equal interval in $\log \sigma$. The larger diamonds represent the more massive galaxies with larger σ . The bins do not include galaxies which lie outside the model grids. For comparison, we also include Globular Clusters from Cenarro et al. (2007) as the grey triangles.

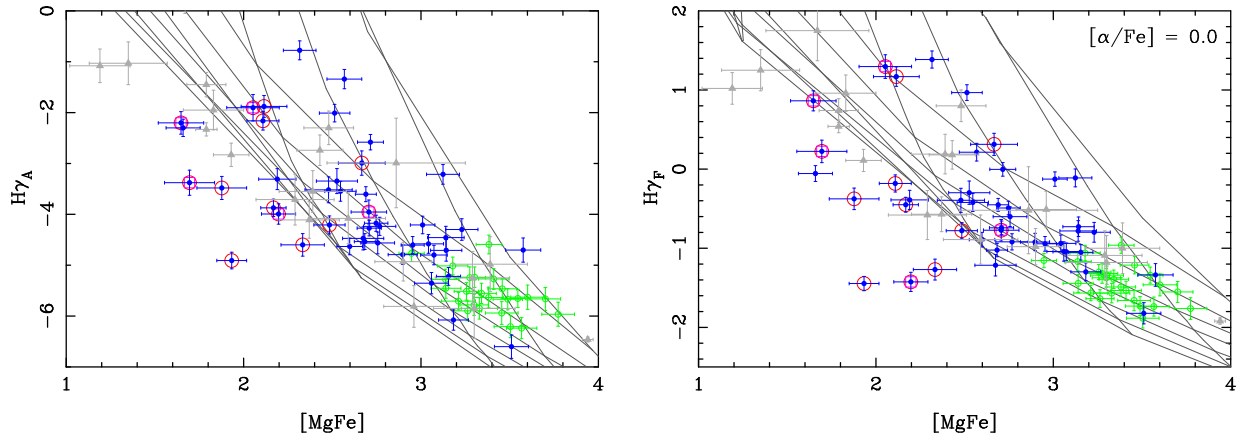


Fig. 6.— $[MgFe]'$ vs. $H\gamma_A$ and $H\gamma_F$ plots. The low- and high- σ galaxies are represented by the blue solid and green open circles, respectively and Globular Clusters by grey triangles. We mark galaxies which are not fitted by the models from Figure 5 with red open circles.

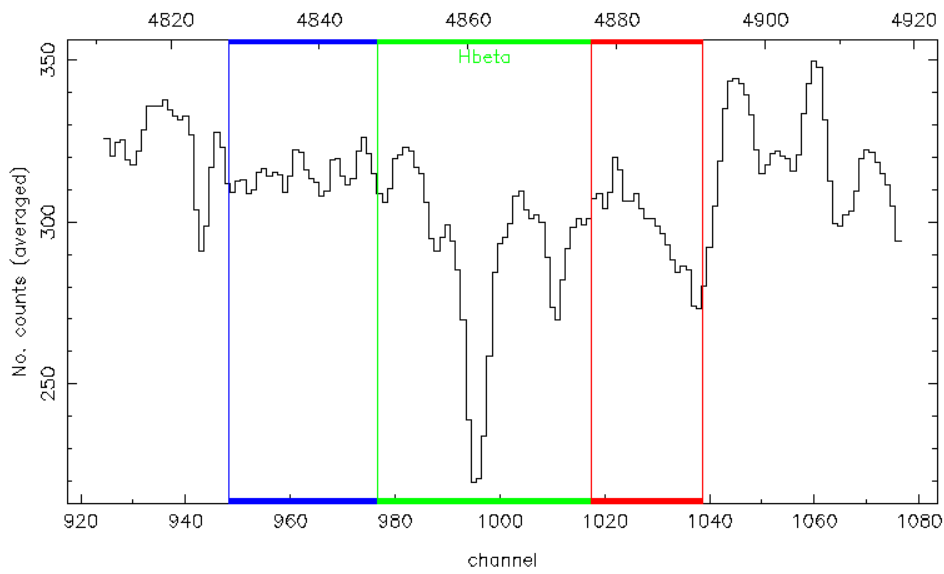


Fig. 7.— $H\beta$ of the off-grid galaxies combined. We stacked the spectra of 13 galaxies which did not fit on the models for $[MgFe]'$ vs. $H\beta$ plot.

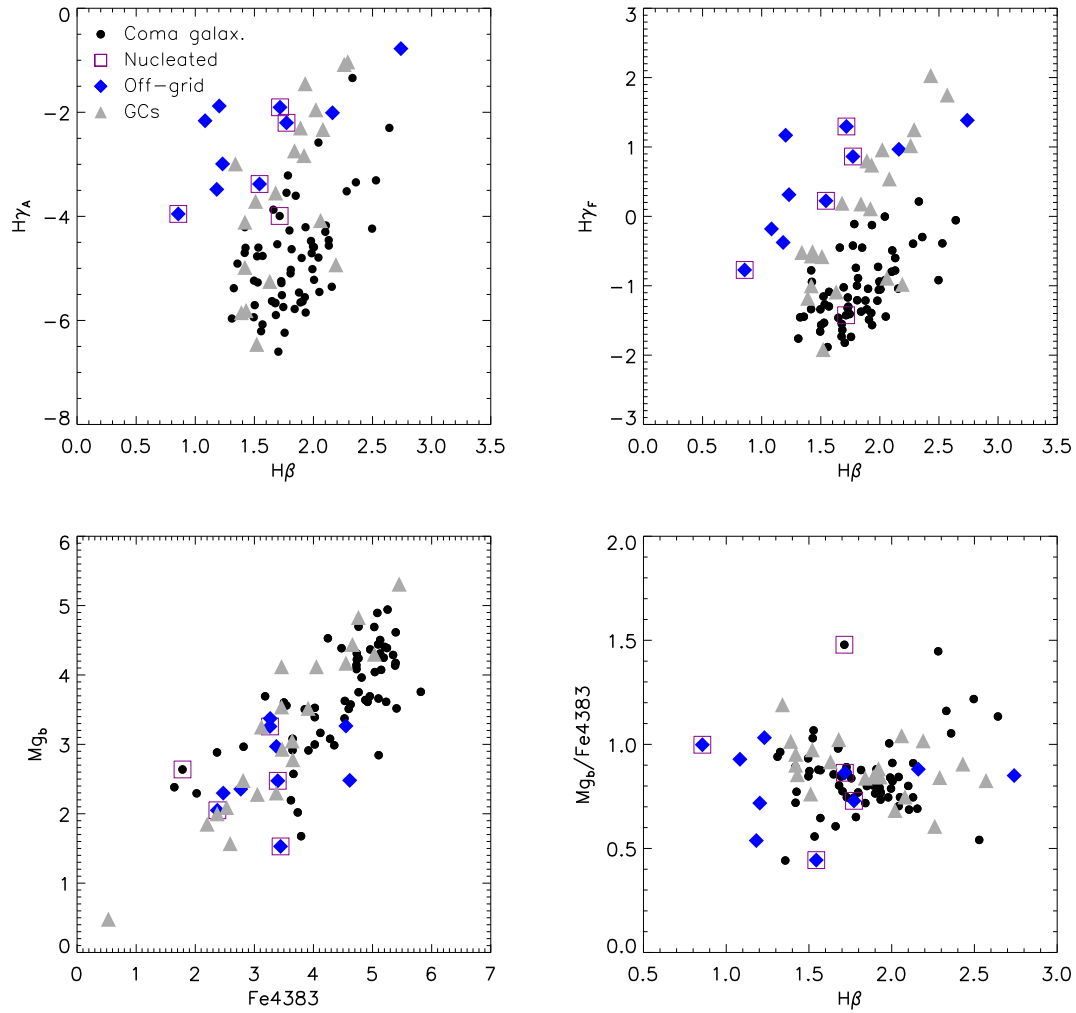


Fig. 8.— Testing the off-grid galaxies. The top left and right plots show H β index vs. the higher order Balmer lines H γ_A and H γ_F . The bottom plots investigate whether there are any inconsistencies in the [Mg/Fe] between the off-grid galaxies with the other galaxies in the sample and GCs (Cenarro et al. 2007). The black filled circles represent the Coma galaxies from our sample where the blue diamonds are off-grid galaxies. Nucleated dEs are marked by purple open squares and the GCs by grey triangles.

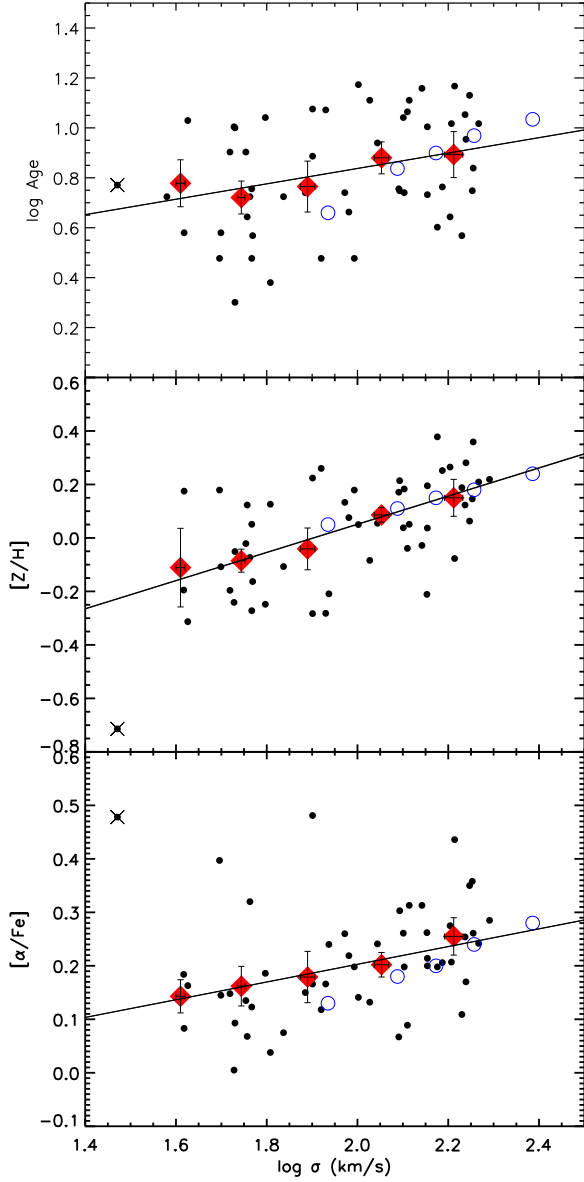


Fig. 9.— $\log \sigma$ versus Age, Metallicity and $[\alpha/\text{Fe}]$ (from top to bottom). The small filled circles are individual galaxies in our data set, red diamonds represent “average” galaxies whose indices were binned by velocity dispersion prior to deriving the SPM parameters, and the blue open circles represent the NFPS data without any offsets applied.

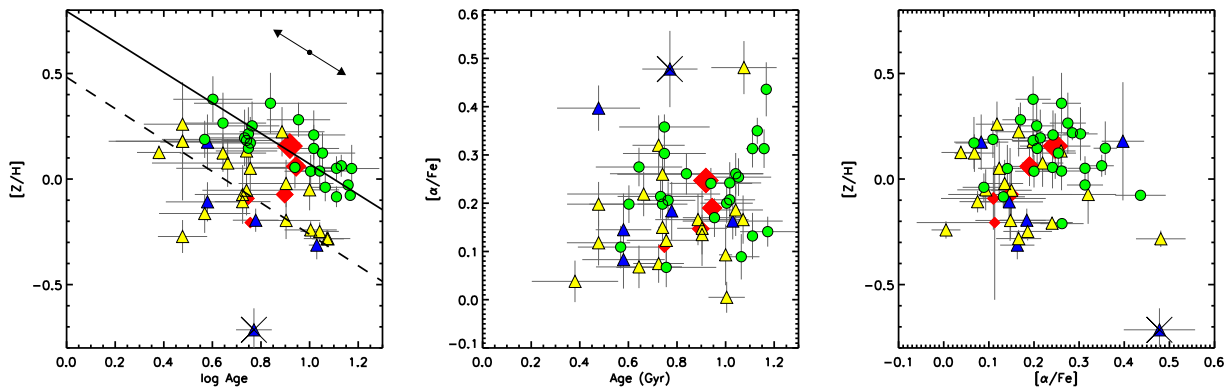


Fig. 10.— Metallicity vs. age, $[\alpha/\text{Fe}]$ vs. age, and metallicity vs. $[\alpha/\text{Fe}]$ for individual galaxies. The green circles represent galaxies with $100 \leq \sigma < 185$ km/s; the yellow triangles mark the galaxies with $50 \leq \sigma < 100$; and the blue triangles are galaxies with $30 \leq \sigma < 50$. The linear fit (left panel) for the high- σ galaxies is marked with a solid line, while the fit to the low- σ galaxies ($\sigma < 100$ km s $^{-1}$) is marked by a dashed line. We excluded the galaxy with the lowest metallicity from the linear regression (it is marked with a cross). The arrows in the top right corner of the age-metallicity plot represent the average correlated error ellipse for age and metallicity. The arrows in the age-metallicity plot represent 1σ correlated error.